



LUND UNIVERSITY

Photon Upconversion in Heavily Doped Semiconductors

Mergenthaler, Kilian

2016

[Link to publication](#)

Citation for published version (APA):

Mergenthaler, K. (2016). *Photon Upconversion in Heavily Doped Semiconductors*. [Doctoral Thesis (compilation), Solid State Physics].

Total number of authors:

1

General rights

Unless other specific re-use rights are stated the following general rights apply:

Copyright and moral rights for the publications made accessible in the public portal are retained by the authors and/or other copyright owners and it is a condition of accessing publications that users recognise and abide by the legal requirements associated with these rights.

- Users may download and print one copy of any publication from the public portal for the purpose of private study or research.
- You may not further distribute the material or use it for any profit-making activity or commercial gain
- You may freely distribute the URL identifying the publication in the public portal

Read more about Creative commons licenses: <https://creativecommons.org/licenses/>

Take down policy

If you believe that this document breaches copyright please contact us providing details, and we will remove access to the work immediately and investigate your claim.

LUND UNIVERSITY

PO Box 117
221 00 Lund
+46 46-222 00 00

PHOTON UPCONVERSION IN HEAVILY DOPED SEMICONDUCTORS

KILIAN MERGENTHALER

DOCTORAL THESIS
2016



LUND
UNIVERSITY

Division of Solid State Physics
Department of Physics
Lund University
Box 118
SE-221 00 Lund
Sweden

THESIS FOR THE DEGREE OF DOCTOR OF PHILOSOPHY

PHOTON UPCONVERSION IN HEAVILY DOPED SEMICONDUCTORS

KILIAN MERGENTHALER

DIVISION OF SOLID STATE PHYSICS
DEPARTMENT OF PHYSICS
LUND UNIVERSITY
SWEDEN



LUND
UNIVERSITY

FACULTY OPPONENT: PROF. DR. SVEN HÖFLING
CHAIR FOR APPLIED PHYSICS
UNIVERSITÄT WÜRZBURG
WÜRZBURG, GERMANY

DOCTORAL THESIS

WHICH, BY DUE PERMISSION OF THE FACULTY OF ENGINEERING AT LUND UNIVERSITY, WILL BE PUBLICLY DEFENDED ON FRIDAY, APRIL 29, 2016, AT 9:30 IN RYDBERG HALL AT THE DEPARTMENT OF PHYSICS, SÖLVEGATAN 14C, LUND.

Front and back cover: Artistically modified photon energy contour plot of n-doped bulk InP measured at 300 K. The original image is shown in Figure 4.13 (c).

Photon Upconversion in Heavily Doped Semiconductors

Thesis for the Degree of Doctor of Philosophy

©2016 Kilian Mergenthaler

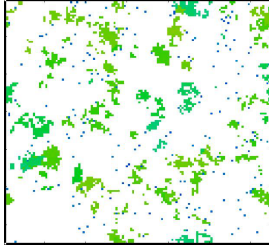
Printed in 2016 by Media-Tryck, Lunds Universitet, Lund, Sweden.

Division of Solid State Physics
Department of Physics
Lund University
Box 118
SE-221 00 Lund
Sweden

ISBN 978-91-7623-715-1 (Print)

ISBN 978-91-7623-716-8 (Pdf)

Typeset by the author using L^AT_EX 2_ε, version 2009/09/24



Are you alive?

Abstract

In this thesis the luminescence properties of highly doped semiconductors are studied with focus on degenerately n-doped InP. It is demonstrated how photoluminescence measurements on degenerately doped semiconductors allow an estimation of the doping concentration without need for electrical contacts. The degenerate doping can furthermore reveal the conduction band structure for energies higher than the bandgap, which is exploited to experimentally support the existence of a theoretically predicted second conduction band minimum in wurtzite InP.

Excitation energy dependence measurements reveal band-to-band absorption for photon energies much lower than the Fermi energy. That absorption causes not only downconverted photoluminescence with photon energies lower than the excitation energy, but also upconverted photoluminescence with photon energies higher than the absorbed laser photon. From the results of the detailed study of this novel upconversion mechanism in degenerately n-doped InP nanowires and bulk InP we propose the following explanation:

An elevated electron gas temperature in degenerately doped semiconductors allows absorption of photon with energies much lower than the Fermi energy. Band-to-band absorption of photons with energies lower than the Fermi energy excites holes with k -values lower than k_F and scattering of the photexcited holes to higher k -values allows \mathbf{k} -conserving radiative recombinations with photon energies higher than the energy of the absorbed photon.

Similar upconversion luminescence is observed for degenerately n-doped bulk GaAs and degenerately p-doped GaAs nanowires, which suggest that similar photon upconversion could be observed in many degenerately doped direct band semiconductors.

The three most important findings about degenerately doped direct band semiconductors are. There is significant photon upconversion for excitation energies between E_g and E_F . The charge carrier recombination rate is higher than, or comparable to the scattering rate of the minority carriers. And, the radiative recombination is strongly dominated by \mathbf{k} -conserving vertical transitions in contrast to the common assumption of relaxation of the \mathbf{k} -selection rule in degenerately doped material.

Popular Science Description

Imagine a solar powered flash light. Each photon absorbed by the flash light's solar cell creates electric energy and the flash light's light source converts the electrical energy again into photons. The purpose of such a device may be questionable, because you would be surprised if it would create more light than what it absorbs. However, under certain conditions it is possible that an absorbed photon creates two or more photons or that an absorbed photon creates a photon with a higher energy.

That one absorbed photon can cause the emission of two (or more) photons is not very surprising, as long as the total energy of the emitted photons is less or equal to the energy of the absorbed photon. It is more surprising if the emitted photon has more energy than the absorbed photon and that is what is studied in this work.

Photon downconversion and upconversion

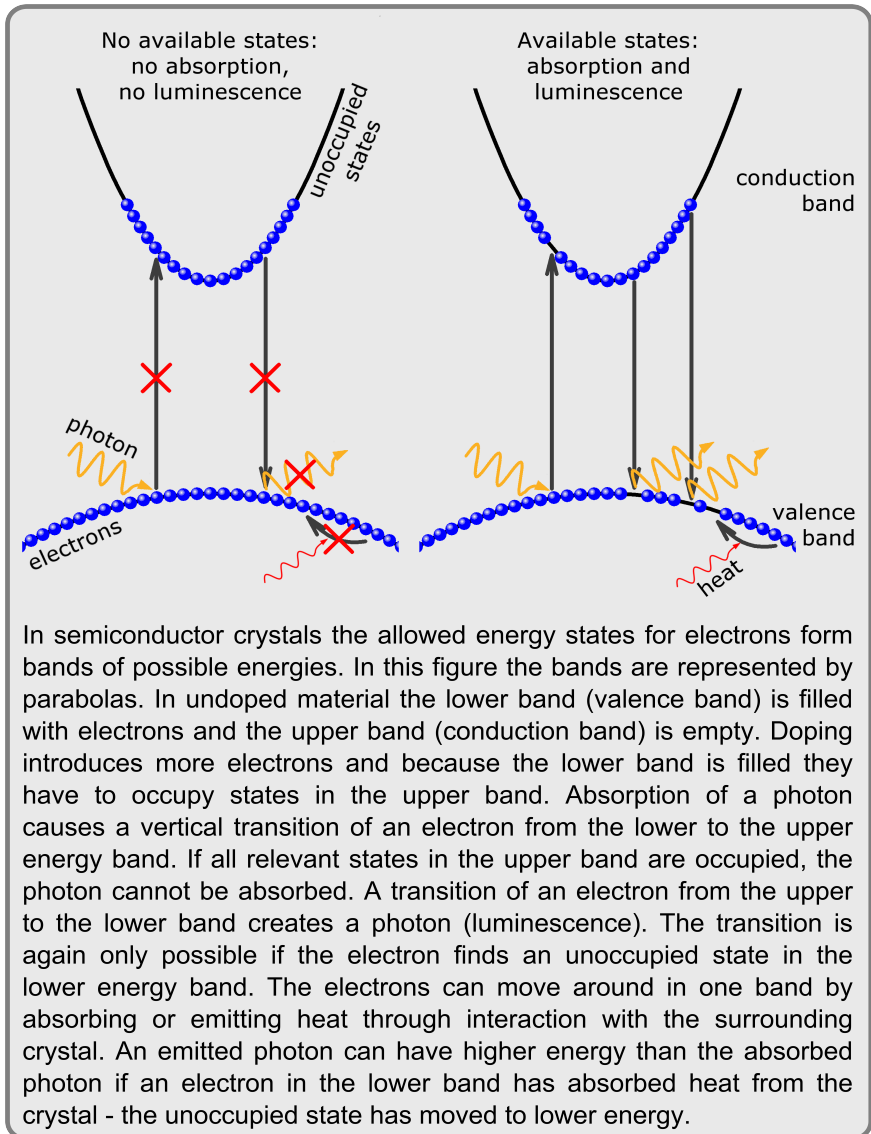
Instead of a solar powered flash light I studied the light emitted by a sample after absorption of photons, a method, which is called photoluminescence. If the emitted photons have lower energy than the absorbed photons (which is typically the case) the process is called photon downconversion. If the emitted photons have higher energy than the absorbed photons the process is called photon upconversion.

One possible mechanism for photon upconversion is the simultaneous absorption of two photons, called two-photon absorption, followed by emission of one photon with the combined energy of both photons. The probability of simultaneous absorption of two or more photons depends strongly on the light intensity hitting the sample. For low light intensities the probability is very low.

Rather Simple Experiment

I was quite surprised when I observed photon upconversion for the first time, because I used relatively low laser light intensities and could exclude two-photon absorption as main upconversion mechanism. I was studying the photoluminescence of doped InP nanowires when I detected photons with energies higher than the laser photon energy. The experiment is rather simple, but apparently nobody before has studied photon upconversion in highly doped semiconductors.

InP is a direct semiconductor, which means it absorbs light much stronger than the indirect silicon. Each semiconductor has a certain photon energy



range where it most efficiently converts absorbed photons into electric energy. Thus, to make a very efficient solar cell, different materials need to be combined. Nanowires are very small structures, only up to one tenth of a micrometer in diameter and a couple of micrometers long. At such small dimensions it is possible to combine the very different semiconducting materials necessary for highly efficient solar cells.

Doping of Semiconductors

Pure semiconductors have quite high electric resistances, but incorporation of specific atoms into the crystal may change the local conductance dramatically. Such incorporation is called doping. Most electronic devices would not work without doping. In the studied sample the InP was doped with sulfur, which means some of the phosphorus atoms in InP were replaced by sulfur atoms. The sulfur atoms have one electron more than the phosphorus atoms and every additional electron increases the electronic conductance.

If the concentration of electrons is sufficiently high they can be treated as an ensemble of particles with average kinetic energy and temperature. The thermal energy of such an electron gas can increase the energy of an emitted photon. However, in my experiments the emitted photon energy was more than the thermal energy higher than the absorbed photon energy. To explain the observed upconversion we have to consider that electrons are Fermions and thus follow the Pauli exclusion principle, which means if two electrons have otherwise identical quantum states they cannot have the same energy.

Electrons are Fermions

If more electrons are added to the system, the additional electrons will occupy higher energy states. The electrons always try to minimize their energy, but if the electrons are heated from the surrounding crystal or external sources they can gain energy if the final state is not already occupied by an electron. Such additional heating of the electrons together with the Pauli exclusion principle can explain the observed upconversion.

The upconversion mechanism I discovered, will not enable perpetual motion or a solar powered flash light with a higher light output power than light input power, however, it may be relevant for future optoelectronic devices. In the present experiments it has proven to allow new ways to study the processes preceding the emission of a photon and how the electrons interact with the surrounding material.

List of Publications

This thesis is based on the work presented in the following papers, which will be referred to by their roman numerals in the text. All material from the papers is reproduced by permission of the respective publisher.

I. Probing the Wurtzite Conduction Band Structure Using State Filling in Highly Doped InP Nanowires

Jesper Wallentin, *Kilian Mergenthaler*, Martin Ek, L. Reine Wallenberg, Lars Samuelson, Knut Deppert, Mats-Erik Pistol, and Magnus T. Borgström

Nano Letters **11**, 2286-2290 (2011)

I performed the optical measurements, took part in the discussion and wrote parts of the paper.

II. Large Energy-Shift Photon Upconversion in Degenerately Doped InP Nanowires by Direct Excitation into the Electron Gas

Kilian Mergenthaler, Azhar Iqbal, Jesper Wallentin, Sebastian Lehmann, Magnus T. Borgström, Lars Samuelson, Arkady Yartsev, and Mats-Erik Pistol

Nano Research **10**, 752-757 (2013)

I performed the continuous wave measurements and was responsible for the development of the theory and for writing the paper.

III. Photon Upconversion in Degenerately Sulfur Doped InP Nanowires

Kilian Mergenthaler, Sebastian Lehmann, Jesper Wallentin, Wei Zhang, Magnus T. Borgström, Arkady Yartsev, and Mats-Erik Pistol

Nanoscale **7**, 20503-20509 (2015)

I performed the measurements and was responsible for the development of the theory and for writing the paper.

IV. Photon Upconversion in Heavily Doped Bulk Semiconductors

Kilian Mergenthaler, Nicklas Anttu, Neimantas Vainorius, Mahtab Ag-haeipour, Sebastian Lehmann, Magnus T. Borgström, Lars Samuelson, and Mats-Erik Pistol

Manuscript

I performed the measurements and was responsible for the development of the theory and for writing the paper.

Publications not included in this thesis:

i **Zn-Doping of GaAs Nanowires Grown by Aerotaxy**

Fangfang Yang, Maria E. Messing, *Kilian Mergenthaler*, Masoomah Ghasemi, Jonas Johansson, L. Reine Wallenberg, Mats-Erik Pistol, Knut Depert, Lars Samuelson, Martin H. Magnusson
Journal of Crystal Growth **414**, 181-186 (2015)

ii **Carrier Recombination Dynamics in Sulfur Doped InP Nanowires**

Wei Zhang, Sebastian Lehmann, *Kilian Mergenthaler*, Jesper Wallentin, Magnus T. Borgström, Mats-Erik Pistol and Arkady Yartsev
Nano Letters **15 (11)**, 7238-7244 (2015)

iii **In Situ Etching for Control Over Axial and Radial III-V Nanowire Growth Rates Using HBr**

Alexander Berg, *Kilian Mergenthaler*, Martin Ek, Mats-Erik Pistol, L. Reine Wallenberg, Magnus T. Borgström
Nanotechnology **25 (50)**, 505601 (2014)

iv **GaAs/AlGaAs Heterostructure Nanowires Studied by Cathodoluminescence**

Jessica Bolinsson, Martin Ek, Johanna Trägårdh, *Kilian Mergenthaler*, Daniel Jacobsson, Mats-Erik Pistol, Lars Samuelson, Anders Gustafsson
Nano Research **4 (7)**, 473-490 (2014)

- v **Semiconductor-Oxide Heterostructured Nanowires Using Postgrowth Oxidation**
Jesper Wallentin, Martin Ek, Neimantas Vainorius, *Kilian Mergenthaler*, Lars Samuelson, Mats-Erik Pistol, L. Reine Wallenberg, Magnus T. Borgström
Nano Letters **13** (12), 5961-5966 (2013)
- vi **Single GaInP Nanowire p-i-n Junctions Near the Direct to Indirect Bandgap Crossover Point**
Jesper Wallentin, Laura Barrutia Poncela, Anna M. Jansson, *Kilian Mergenthaler*, Martin Ek, Daniel Jacobsson, L. Reine Wallenberg, Knut Depert, Lars Samuelson, Dan Hessman, Magnus T. Borgström
Applied Physics Letters **100** (25), 251103 (2012)
- vii **Numerical Simulations of Absorption Properties of InP Nanowires for Solar Cell Applications**
Peter Kailuweit, Marius Peters, Jack Leene, *Kilian Mergenthaler*, Frank Dimroth, Andreas W. Bett
Progress in Photovoltaics **20** (8), 945-953 (2012)
- viii **Fabrication and Characterization of AlP-GaP Core-Shell Nanowires**
Magnus T. Borgström, *Kilian Mergenthaler*, Maria E. Messing, Ulf Håkanson, Jesper Wallentin, Lars Samuelson, Mats-Erik Pistol
Journal of Crystal Growth **324** (1), 290-295 (2011)
- ix **A New Route Toward Semiconductor Nanospintronics: Highly Mn-Doped GaAs Nanowires Realized by Ion-Implantation Under Dynamic Annealing Conditions**
Christian Borschel, Maria E. Messing, Magnus T. Borgström, Waldomiro Paschoal Jr., Jesper Wallentin, Sandeep Kumar, *Kilian Mergenthaler*, Knut Deppert, Carlo M. Canali, Håkan Pettersson, Lars Samuelson, and Carsten Ronning
Nano Letters **11** (9), 3935-3940 (2011)
- x **Diffusion Length Measurements in Axial and Radial Heterostructured Nanowires Using Cathodoluminescence**
Jessica Bolinsson, *Kilian Mergenthaler*, Lars Samuelson, Anders Gustafsson
Journal of Crystal Growth **315** (1), 138-142 (2011)

- xi **Growth of β -Ga₂O₃ on Al₂O₃ and GaAs Using Metal-Organic Vapor-Phase Epitaxy**
Volker Gottschalch, *Kilian Mergenthaler*, Gerald Wagner, Jens Bauer, Hendrik Paetzelt, Chris Sturm, Ulrike Teschner
phys. stat. sol. (a) **206**, 243-249 (2009)
- xii **Growth and Characterization of ZnO Nanostructures on Sapphire Substrates**
Kilian Mergenthaler, Volker Gottschalch, Jens Bauer, Hendrik Paetzelt and Gerald Wagner
Journal of Crystal Growth **310**, 5134-5138 (2008)

Contents

1	Introduction	1
2	Theoretical Background	5
2.1	Absorption in Semiconductors	5
2.2	Burstein-Moss Shift	7
2.3	Absorption Below E_F	11
2.4	Photoluminescence Intensity	13
2.5	Photon Upconversion	14
2.6	Carrier Scattering in Semiconductors	17
3	Experimental Details	23
3.1	Crystal Growth	23
3.2	Nanowire Growth	24
3.3	Single Nanowire Measurements	25
3.4	Photoluminescence Spectroscopy	27
3.5	Photoluminescence Excitation Spectroscopy	29
3.6	Cross-Polarized Dark Field Spectroscopy	30
4	Results	33
4.1	Probing the Conduction Band Structure	33
4.2	Electron Gas Temperature	38
4.3	Photon Downconversion	45
4.4	Photon Upconversion in n-doped InP	49
4.5	Photon Upconversion in GaAs	56
5	Conclusion and Outlook	59
	Acknowledgements	63
	Bibliography	65

Contents

Paper I: Probing the Wurtzite Conduction Band Structure Using State Filling in Highly Doped InP Nanowires	74
Paper II: Large-Energy-Shift Photon Upconversion in Degenerately Doped InP Nanowires by Direct Excitation Into the Electron Gas	82
Paper III: Photon Upconversion in Degenerately Sulfur Doped InP Nanowires	91
Paper IV: Photon Upconversion in Degenerately Doped Bulk InP	100

Chapter 1

Introduction

"I have never had a single positive doping test."

Lance Armstrong, January 2004

Semiconductor devices are omnipresent in our digitalized world and almost all devices require doped semiconducting material. The most common electronic device is the transistor and other examples are solar cells and light emitting diodes (LEDs), all of which rely on highly doped semiconductors.

In recent decades the need for more transistors per integrated circuit caused a technological progression to smaller and smaller transistor dimensions and since about 2005 the active device size is smaller than 100 nm [1]. A transition to devices composed of nanometer sized elements may also be advantageous for solar cells [2, 3] and light emitting diodes [4, 5]. One advantage is the up to 20 times higher absorption per semiconductor volume in ordered nanowire arrays compared to bulk material [2].

Very promising for applications are alloy semiconductor nanowires composed of group III and group V elements of the periodic table. In contrast to silicon, most III-V semiconductors have a direct bandgap, which causes more efficient absorption and emission of photons and the small diameter of nanowires allows combinations of materials with very different lattice constants [6]. Such combinations are relevant for efficient multi-junction solar cells, where each junction is optimized for absorption of a specific wavelength range.

For optoelectronic devices, such as solar cells and LEDs, the optical properties of the material are of major importance. A very specific optical property is photon upconversion, which is a summarizing term for all processes which convert absorbed photons into photons with higher energy than the absorbed photons. Photon upconversion has many different applications ranging from

Chapter 1: Introduction

medicine and biology to optoelectronics and photonics [7–11].

Photon upconversion in semiconductors has been reported for quantum dots [12, 13], for type II heterojunctions and quantum wells [14, 15], and for the high bandgap materials GaN and ZnO [16, 17]. Despite an extensive literature search and despite the technological importance of highly doped semiconductors we have found no previous reports on photon upconversion in degenerately doped semiconductors. Thus the main finding of this work is the observation of photon upconversion in degenerately doped direct bandgap III-V semiconductors.

For this work the optical properties of n-doped InP nanowires were studied to evaluate doping concentration, crystal structure and possible application in nanowire solar cells. The results show that sulfur doping of InP nanowires may change the crystal structure from zincblende to wurtzite, where the latter is a phase not stable in bulk growth processes. Furthermore, we show that photoluminescence can be used to probe the conduction band structure of degenerately doped material, which is especially relevant for wurtzite as relatively new material.

For excitation energies above the bandgap but lower than the Fermi energy of the degenerately doped InP nanowires, we observed photon upconversion. Our results of similar measurements on n-doped bulk InP, n-doped bulk GaAs and p-doped GaAs nanowires show that the observed upconversion is not limited to InP nor to nanowires or n-doping. Our model of the upconversion mechanism includes an elevated temperature of the majority carriers and scattering of the photoexcited minority carrier to higher k -values. Most parts of this work have already been published in peer reviewed journals as can be seen in the list of papers.

In Chapter 2 of this thesis I introduce the theoretical background. The chapter includes a description of the Burstein-Moss state filling, absorption into a heated electron gas and an explanation of different photon upconversion mechanisms.

In Chapter 3 the experimental details are presented such as crystal growth, nanowire growth and sample preparation. The spectroscopy methods photoluminescence (PL), photoluminescence excitation spectroscopy (PLE) and cross-polarized dark field PL are described, including a description of the measurement setups.

The Results in Chapter 4 are divided into five parts. The first part is based on Paper I and describes how the doping concentration can be calculated from the luminescence spectra and how through the state filling the conduction band structure can be probed. The second part is based on Paper II and

III and discusses heating of the electron gas. In the third and forth part I compare the photon downconversion and upconversion results of the n-doped InP nanowires (Paper II and III) with the results on n-doped bulk InP (Paper IV). The fifth part shows the results of degenerately n-doped bulk GaAs and degenerately p-doped GaAs nanowires.

Chapter 5 concludes and summarizes the thesis.

Chapter 2

Theoretical Background

*"There can be no flight without preceding dreams of flying."
Stanisław Lem in "Golem XIV"*

The optical properties of a material describe how photons interact with the material, which includes reflection, transmission, absorption and reemission of photons. If a light beam hits a sample, a fraction of it is reflected at the surface, a fraction may be absorbed, and the rest is transmitted. Semiconductors can be defined as materials with an optical bandgap between zero and about 4 eV [18]. Almost all photons with energies lower than the bandgap will be transmitted and most photons with energies higher than the bandgap will be absorbed. Most photons emitted by a semiconductor will have energies equal to the bandgap energy. Those optical properties of semiconductors are the basis of many of their important optical applications, such as lasers, light emitting diodes, photodetectors and solar cells.

A second way to define a semiconductor is as a material with electrical resistivity in the range of $10^{-3} \Omega\text{cm}$ to $10^8 \Omega\text{cm}$ [19]. However, the resistivity of a semiconductor can easily be changed through the incorporation of defect atoms. Such doping of semiconductors is required for almost all electronic devices. In this work the optical properties of highly doped semiconductors were studied with a focus on the light reemitted after absorption of photons, the photoluminescence.

2.1 Absorption in Semiconductors

In semiconductors only photons with sufficient energy can excite electrons from the filled valence bands to the empty conduction bands. Most photons

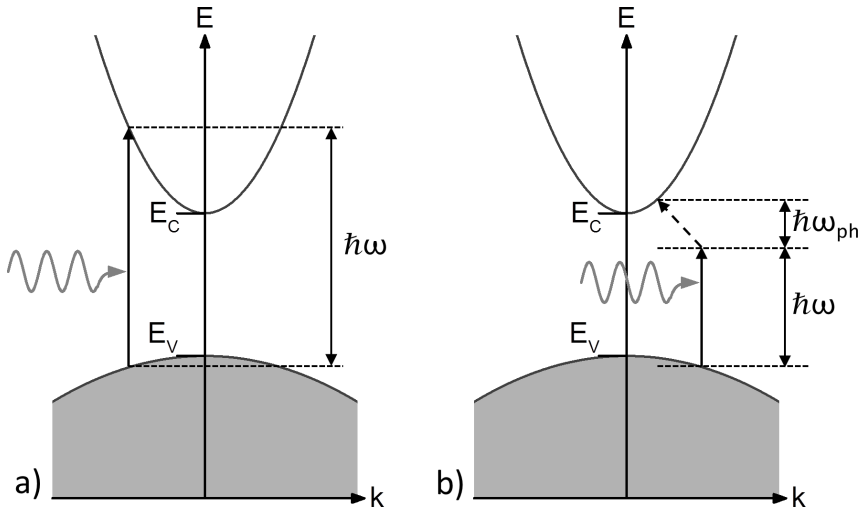


Figure 2.1: Schematic images of direct (a) and indirect absorption (b) in a direct bandgap semiconductor. Grey areas indicate filled states.

with energy less than the bandgap are transmitted. The bandgap is the energy separation between the highest valence band state (E_V) and the lowest conduction band state (E_C) and is usually denoted as E_g . The bandgap is a material specific value, which depends amongst others on the material composition, the crystal structure, and the temperature.

The energy of an absorbed photon is transferred to an electron by lifting the electron to a higher energy state. The energy transfer is only possible if the process is momentum conserving (k -conserving). Due to the comparably low momentum of photons the absorption process leaves the momentum of the electron almost unchanged and the electron can only be excited to states with similar k . Such a vertical transitions in k -space, which is also called a direct transition, is shown in Figure 2.1 (a). k -indirect transitions, where the initial and the final electron state have different k -values (see Fig. 2.1 (b)) are only allowed if the momentum difference is contributed by interaction with a third (quasi) particle, for example with lattice vibrations, also known as phonons. A phonon can provide momentum to the electron and additionally contributes a small amount of energy, marked as $\hbar\omega_{ph}$ in Figure 2.1 (b). Such indirect transitions allow absorption already at an energy of $E_g - \hbar\omega_{ph}$. However, the probability of simultaneous absorption of a photon and emission or

absorption of a phonon is about 10^{-3} compared to the direct transitions without phonon contribution [20].

Indirect transitions play an important role in indirect semiconductors, such as silicon and germanium, where the top of the valence band and the bottom of the conduction band are not at the same position in \mathbf{k} -space, and thus, excitation to the lowest conduction band state requires phonon assisted absorption.

In this work InP and GaAs were studied, which are both direct semiconductors since the top of the valence band and the bottom of the conduction band are at the same position in \mathbf{k} -space (at the Γ -point). Direct bandgap materials are beneficial for optoelectronic devices since the absorption and emission of light is much stronger than for indirect materials. For example are most solar cells made of the indirect semiconductor silicon typically hundreds of micrometers thick to absorb sufficient light whereas in direct bandgap material less than one micrometer of active material is sufficient [2].

2.2 Burstein-Moss Shift

In 1954 Elias Burstein measured the absorption of highly n-doped InSb and observed for increasing doping concentrations a shift of the absorption edge to higher energies [21]. The effect was explained by Trevor Simpson Moss the same year as a result of state filling in the conduction band [22]. In degenerately doped semiconductors all states close to the conduction band edge are populated and therefore no transition to these states can take place. This shift of the absorption edge is depicted schematically in Figure 2.2. For a given temperature T , about $4k_B T$ below the Fermi energy more than 98 % of the states are populated and absorption starts around $\hbar\omega = E_F - 4k_B T$, where k_B denotes the Boltzmann constant and E_F the Fermi energy.

For free electrons the energy-wavevector relation can be written as $E = \hbar^2 k^2 / 2m$, thus the reciprocal mass ($1/m$) determines the curvature of the energy dispersion. For an arbitrary dispersion the relation can be generalized to define the effective mass tensor in a material as

$$(m^{-1})_{ij} = \frac{1}{\hbar^2} \frac{\partial^2 E}{\partial k_i \partial k_j}. \quad (2.1)$$

Close to the Γ -point the energy-momentum relations of conduction band and valence band are parabolic and isotropic and the dependence simplifies to $E = \hbar^2 k^2 / 2m_{e,h}$. The indices e and h indicate the conduction band mass

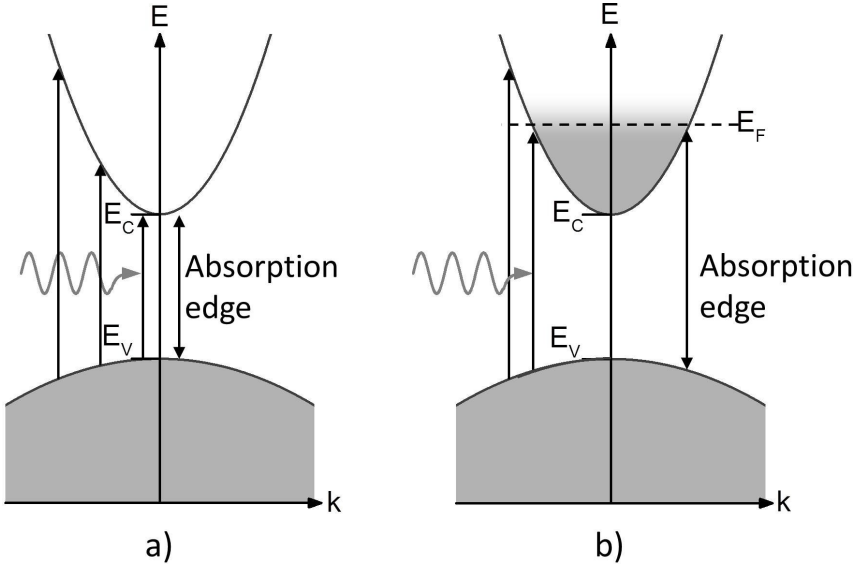


Figure 2.2: Schematic images of the absorption edge dependence on state filling: a) undoped and b) degenerately doped semiconductor material. Grey areas indicate filled states.

of an electron and the valence band mass of a hole, respectively. A hole is defined as a missing electron in an otherwise filled band with $\mathbf{k}_h = -\mathbf{k}_e$, $E_h(\mathbf{k}_h) = -E_e(\mathbf{k}_e)$ and $m_h = -m_e$ [20].

With that concept of electron and hole mass, for parabolic bands and \mathbf{k} -conserving optical transitions the absorption in degenerately doped semiconductors starts around

$$\hbar\omega = E_g + \frac{\hbar^2 \hat{k}^2}{2m_e} + \frac{\hbar^2 \hat{k}^2}{2m_h} - 4k_B T, \quad (2.2)$$

where \hat{k} denotes the \mathbf{k} -value of the lowest energy transitions. The respective energy shift in the conduction band and valence band are then equal to

$$\Delta E_C = \frac{\hbar^2 \hat{k}^2}{2m_e} \quad \text{and} \quad \Delta E_V = \frac{\hbar^2 \hat{k}^2}{2m_h}. \quad (2.3)$$

2.2 Burstein-Moss Shift

The measured shift of the absorption edge $\Delta E = \Delta E_C + \Delta E_V = \hbar\omega - E_g$ depends on the state filling in the respective band and can be used to determine the doping concentration. In the following, I will derive the dependence for degenerate n-doping and filling of the conduction band with electrons, but a similar dependence can be derived for p-doping and filling of the valence band with holes.

To get the relation between energy shift and carrier concentration the density of electrons in the conduction band needs to be calculated:

$$n = \int_{E_C}^{\infty} D_e(E) f_e(E) dE, \quad (2.4)$$

where D_e is the density of electron states and f_e the Fermi-Dirac distribution. The Fermi-Dirac distribution

$$f_e(E, T) = \frac{1}{\exp \frac{E - E_F}{k_B T} + 1}, \quad (2.5)$$

gives the probability that for temperature T a state at energy E is occupied. For undoped material and low doping concentrations, the probability that a conduction band state is populated, is low and the Boltzmann approximation $f_e \approx \exp[-(E - E_F)/(k_B T)]$ can be used and the integral in Eq. 2.4 can easily be executed, but not for a degenerately doped semiconductor. Generally the electron density n is given by

$$n = 2 \left(\frac{m_e k_B T}{2\pi \hbar^2} \right)^{3/2} F_{1/2} \left(\frac{E_F - E_C}{k_B T} \right), \quad (2.6)$$

where $F_n(x)$ is the Fermi integral which is defined as

$$F_n(x) = \frac{2}{\sqrt{\pi}} \int_0^{\infty} \frac{y^n}{1 + \exp(y - x)} dy. \quad (2.7)$$

For $x \gg 1$, i.e. $E_F - E_C \gg k_B T$ the Fermi integral can be approximated by $2\sqrt{\pi}(2/3)x^{3/2}$ and due to the assumption of low temperature the summand $4k_B T$ can be neglected. Thus the relation between electron concentration and energy shift can be written as:

$$\Delta E = \frac{\hbar^2}{2m_{\text{eff}}} (3\pi^2 n)^{2/3}, \quad (2.8)$$

where m_{eff} is the effective mass of the involved electron and hole. This

Chapter 2: Theoretical Background

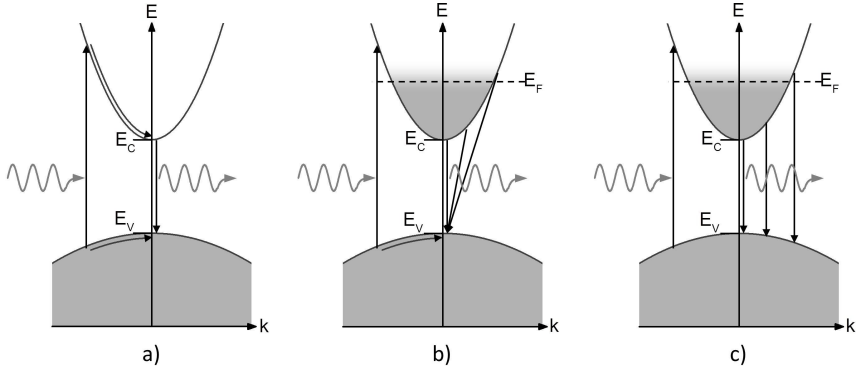


Figure 2.3: Schematic images of the dependence of luminescence on state filling: a) undoped, b) and c) degenerately doped semiconductor material, b) non- \mathbf{k} -conserving recombination and c) \mathbf{k} -conserving recombination. Grey areas indicate filled states.

equation is valid for degenerately p -doped material as well, with hole concentration p instead of the electron concentration as the only difference.

In luminescence measurements on degenerately doped material the high energy side of the luminescence can be used to approximate the position of the Fermi energy and through Eq. 2.8 this shift can be used for an estimation of the charge carrier concentration [23–25].

The effect of state filling on the emission is schematically depicted in Figure 2.3. In undoped direct semiconductors, absorption and recombination processes usually conserve the \mathbf{k} -vector (see Fig. 2.3 (a)). It is possible for electrons and holes with a finite \mathbf{k} -vector to recombine before they relax to their respective band extrema (which has been observed using femtosecond spectroscopy [26]), however, such a recombination is a very unlikely process because it requires holes and electrons with similar \mathbf{k} and $k > 0$.

Many scientific publications have assumed that in degenerately doped semiconductors the \mathbf{k} -conservation rule is relaxed, which means that holes at $\mathbf{k} = 0$ recombine not only with electrons with $\mathbf{k} = 0$, but also with electrons with finite \mathbf{k} -vector (see for example [27–30]). Such indirect, non- \mathbf{k} -conserving recombination is depicted in Figure 2.3 (b). In this work I show experimental evidence that the radiative recombination in degenerately doped semiconductors is dominated by the \mathbf{k} -conserving process shown in Figure 2.3 (c), where hot holes recombine with conduction band

electrons with similar \mathbf{k} -vectors.

The absorption energy shift in equation 2.8 is derived for \mathbf{k} -direct transitions, for \mathbf{k} -indirect transitions it would change to

$$\Delta E = \frac{\hbar^2}{2m_e}(3\pi^2n)^{2/3} \quad \text{and} \quad \Delta E = \frac{\hbar^2}{2m_h}(3\pi^2p)^{2/3} \quad (2.9)$$

for n -doping and p -doping, respectively.

2.3 Absorption Below E_F

The absorption in semiconductors increases strongly for photons with energies larger than the bandgap energy. However, some processes allow also absorption of photons with energies lower than the bandgap. The indirect phonon assisted absorption was already mentioned. Other mechanisms leading to absorption below the bandgap energy are: Excitonic states, transitions involving defect states and free carrier absorption.

An exciton is a hydrogen-like state due to mutual Coulomb interaction between a conduction band electron and a valence band hole. In absorption measurements the exciton is visible as absorption peak close below the bandgap energy. The exciton binding energy in InP is about 4.8 meV [31] and in GaAs about 4.2 meV [32], which corresponds to thermal energies of 56 K and 49 K, respectively. Thus, at room temperature excitonic effects are not observed. In highly doped semiconductors the exciton is unstable due to the screening effect of large carrier concentrations [20].

The term defect state absorption describes transitions from the valence band to a defect state, from a defect state to the conduction band or from an acceptor state to a donor state. For low doping concentration the defect state absorption is visible as sharp peaks below the bandgap energy. For doping concentrations higher than the critical doping concentration (for GaAs about 10^{16} cm^{-3} [33]) an impurity band is formed that eventually overlaps with the conduction or valence band. That overlap fills the conduction or valence band states and leads to degenerate doping of the semiconductor. The many-body Coulomb interaction in highly doped material also leads to narrowing of the observed bandgap, which is called bandgap narrowing or bandgap renormalization.

Free carrier absorption describes intra-band photoexcitation of conduction band electrons or valence band holes. In degenerately doped semiconductors this effect strongly increases the sub-bandgap absorption. However, free

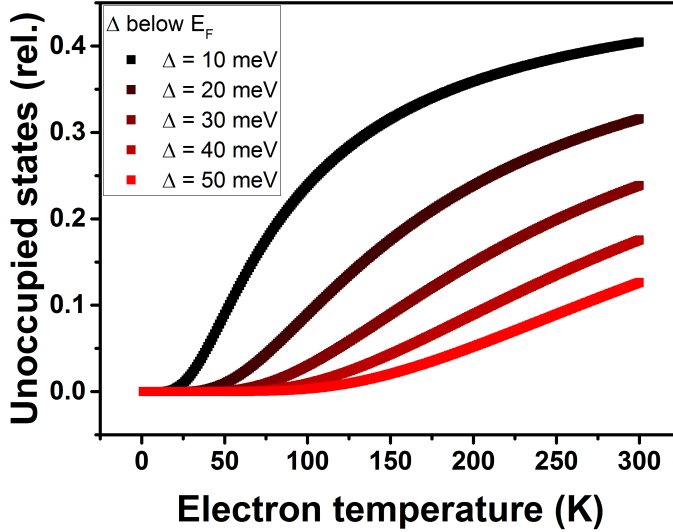


Figure 2.4: Temperature dependence of the fraction of unoccupied states selected energies below the Fermi energy.

carrier absorption does not separate electrons and holes over the band gap and does not lead to radiative recombination.

In real samples the onset of the absorption at the bandgap energy does not follow the theoretical square root dependence of the density of states, instead an exponential tail is observed. This tail is called the Urbach tail [34] and is attributed to deviations from the perfect crystal. The deviations can be caused by defects, doping or fluctuations due to lattice vibrations [20].

In the previous section the absorption edge was derived for degenerately doped semiconductors at low temperatures. For higher temperatures, the elevated temperature of the charge carrier gas allows band-to-band transitions to unoccupied states below the Fermi energy. The temperature dependence of the fraction of unoccupied states at an energy below the Fermi energy is described by the Fermi-Dirac distribution (Eq. 2.5).

Figure 2.4 shows the temperature dependence of the relative number of unoccupied states for selected energies below the Fermi energy. It illustrates that band-to-band absorption into the filled band is only allowed for energies

close to the Fermi energy or elevated temperatures.

2.4 Photoluminescence Intensity

If the absorption of photons leads to conduction band electrons and valence band holes, the electrons and holes can recombine and emit a photon. This process is called photoluminescence (PL). The intensity of the PL signal is proportional to the product of the conduction band electron concentration and the valence band hole concentration [35]. Every electron needs a hole to recombine with. Thus, the integrated PL intensity, which is proportional to the radiative recombination rate, is

$$I_{\text{PL}} = c_a \cdot BN^2, \quad (2.10)$$

where N is the electron-hole concentration, B is a coefficient for band-to-band recombination and c_a a proportionality constant that is determined by sample and measurement geometry.

Under low injection conditions the generation-recombination rates can be written as powers of the electron-hole concentration [36]. The three most important processes are: Intrinsic band-to-band generation-recombination, Shockley-Read-Hall (SRH) generation-recombination and Auger generation-recombination processes.

SRH processes describe non-radiative transitions of charge carriers from or to defect states. Such transitions involve only one charge carrier (and usually a phonon) and thus, their generation-recombination rate is proportional to N . Band-to-band processes involve two charge carriers and have a rate proportional to N^2 . In Auger processes momentum and energy of the recombination of an electron and a hole are transferred to another electron or hole. Those processes involve three charge carriers and thus, their generation-recombination rate is proportional to N^3 .

Hence, the fraction of absorbed excitation intensity is related to the recombination rates by

$$I_{\text{L}} = c_b(AN + BN^2 + CN^3), \quad (2.11)$$

where A , B and C are coefficients for SRH, band-to-band and Auger processes, respectively. c_b is again a sample and measurement specific proportionality constant. By combining Eq. 2.10 and Eq. 2.11 the excitation intensity can be written as powers of the integrated PL intensity

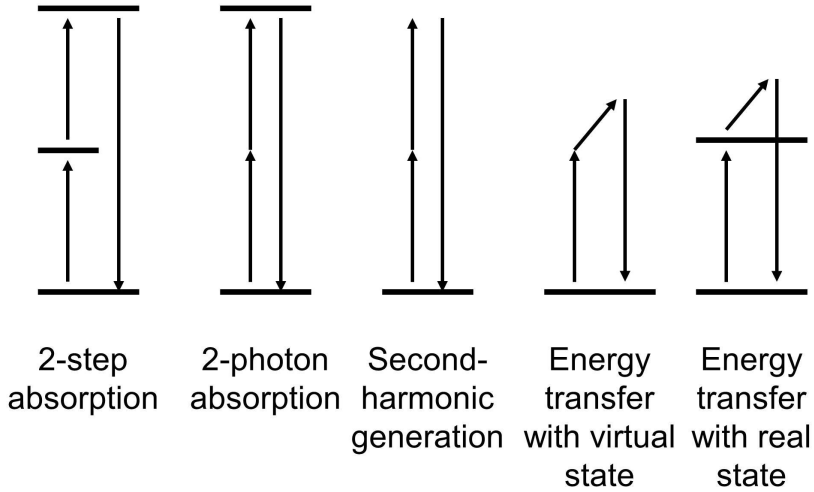


Figure 2.5: A selection of photon upconversion processes.

$$I_L = A_{PL}(I_{PL})^{1/2} + B_{PL} \cdot I_{PL} + C_{PL}(I_{PL})^{3/2}, \quad (2.12)$$

with A_{PL} , B_{PL} and C_{PL} as coefficients for each of the generation-recombination processes. When any one of the processes is dominant, Eq. 2.12 is reduced to a simple power law, with the form $I_{PL} \propto (I_L)^\alpha$, where the exponent α reveals the underlying dominant process: $\alpha < 1$ Auger processes, $\alpha = 1$ band-to-band processes, and $\alpha > 1$ SRH processes.

2.5 Photon Upconversion

For most photoluminescence measurements the photon energy of the exciting laser is chosen to be much higher than the expected emission of the studied material. The spectral response from the sample is then recorded for energies below the laser photon energy and no luminescence is expected above the laser energy. Only under certain conditions photo absorption can lead to the emission of photons with higher energies than the energy of the absorbed photons and all such processes require that the additional energy comes from an energy reservoir, for instance from heat, or from multi photon absorption.

Photon upconversion can occur through many different physical mecha-

2.5 Photon Upconversion

nisms [37], however most mechanisms can be described by one of the processes depicted in Figure 2.5. The first three mechanisms in Figure 2.5 show photon upconversion caused by absorption of two photons. The absorption of two photons can be sequential for instance via electron levels in ions or electronic states in the semiconductor bandgap (Two-step absorption) or it can be simultaneous absorption of two photons [38]. If the simultaneous absorption of two photons excites an electron to a real state it is called two-photon absorption. If the absorption of two photons causes photon upconversion without available real excited states the process is called second-harmonic generation.

The last two mechanisms in Figure 2.5 summarize photon upconversion processes with contribution of other energy sources. The additional energy typically is contributed as heat, for example the temperature of the surrounding crystal, atoms, or electrons, however it can also be contributed by deexcitation of surrounding excited electrons (Auger processes). For photon upconversion caused by thermal excitation the emission energy does not exceed the excitation energy by more than a few $k_B T$ [38]. For photon upconversion through Auger processes the photon energy gain is limited by the energy of the deexcitation process. Both photon upconversion mechanisms can occur with real and with virtual electron states as depicted in Figure 2.5.

The first studied photon upconversion mechanisms were upconversion processes caused by thermal population of energy states above the absorption state [37], one such example is the well-known anti-Stokes emission in Raman spectroscopy [39–41]. As reference to these anti-Stokes Raman lines, photon upconversion luminescence is in general sometimes also called anti-Stokes photoluminescence.

In recent years photon upconversion with more than a few $k_B T$ energy gain has been reported for many different systems and materials:

- For lanthanide and uranide ions embedded in solids [37, 42–44] the strongest upconversion mechanisms are multistep excitations, and energy transfer upconversion. In multistep excitation an excited ion absorbs another photon and in energy transfer upconversion the energy of an excited ion is transferred to a second excited ion.
- Strong upconversion was reported for colloidal [13, 45, 46] and self assembled quantum dots [13, 47, 48], where the photon upconversion was caused by two-step two-photon absorption [12, 13, 45], or by excitation to higher energy states through phonon-assisted excitation [46] or energy transfer from Auger recombination processes [49].

Chapter 2: Theoretical Background

- In two-dimensional hetero-structure quantum well systems the observed upconversion was explained by Auger process excitation of electrons from the well into the barrier material [14, 50–52] or by two-step two-photon absorption [53–56].
- In bulk or bulk-like high bandgap semiconductors such as GaP and ZnO, upconversion was observed for excitation photon energies lower than the bandgap [17, 57, 58]. The observation was explained by second harmonic generation [59–61], by two-step two-photon absorption via defect states [57, 58, 62, 63] or by optical-phonon assisted, below bandgap absorption [64].
- In bulk GaAs and AlGaAs the reported photon upconversion was explained by two-step two-photon absorption via defect states in the bandgap [65–68]. From the literature study, I conclude that so far only intrinsic and lowly doped zincblende III-V semiconductors have been studied for photon upconversion.

For this work I studied photon upconversion in degenerately doped InP and GaAs. I observed photon upconversion for excitation photon energies higher than the bandgap, but lower than the Fermi energy in the studied material. From the analysis of the measured results I conclude that the observed photon upconversion process does not require two-step two-photon absorption nor indirect phonon assisted absorption. Instead I propose an upconversion mechanism relying on band-to-band absorption below the Fermi energy and scattering of the photoexcited minority carrier to higher k -values.

Photon upconversion is not only of scientific interest, but is also of significant technological importance. One example is upconversion lasers, which are a promising approach towards short wavelength, visible, coherent light sources [9, 69] and tunable UV solid-state lasers [37]. A second example is biological imaging [70], where upconversion is of interest due to its low photo-damage to living organisms, weak background fluorescence, high detection sensitivity, and high light-penetration depth in tissues. And, a third example for technical applications of upconversion is the detection of infrared photons where the upconverted radiation may be detected with relatively high sensitivities with no requirement for any cryogenic cooling [8]. Furthermore photon upconversion could be used for optical cooling [71] and to increase solar cell efficiency [62, 63].

2.6 Carrier Scattering in Semiconductors

Only absorption of photon energies equal to the bandgap creates charge carriers at the respective band extremum and absorption of higher energy photons creates charge carriers at higher energies and higher k . To reach the band extremum the charge carriers need to lose the excess energy and momentum via scattering processes. The most important scattering mechanisms in III-V semiconductors are:

- scattering with ionized impurities,
- scattering with acoustical and optical phonons, and
- scattering with other charge carriers.

For low temperatures the scattering with ionized impurities dominates and for high temperatures scattering with polar optical phonons is the dominating scattering process [72]. In degenerately n-doped semiconductors only the relaxation of the photoexcited holes need to be considered and the electron gas can be seen as an ensemble of particles. However, the scattering rates depend not only on many material specific constants, but also on hole energy and sample temperature.

In this section, I will present calculations of the hole energy dependence of the scattering rates of holes in InP, for scattering with ionized impurities and with LO phonons. The calculation is based on the equations presented by Brudevoll et al. [73]. The InP parameters used for the calculation are summarized in Table 2.1.

Scattering of a hole with ionized impurities is treated similar to Rutherford scattering and the scattering rate can be derived by considering singly charged impurities with a screened Coulomb potential. The scattering rate can then be expressed by

$$P^{\text{im}} = \frac{3e^4 N_i m_f F}{32\pi \hbar^3 \epsilon_0^2 \epsilon_S^2 k_i^2 k_f}, \quad (2.13)$$

where e is the electron charge, N_i is the density of ionized scatterers, ϵ_0 is the vacuum dielectric constant, m is the hole mass, and ϵ_S is the static relative dielectric permittivity of the semiconductor. The indices i and f mark initial and final states of the scattering hole. For elastic intraband scattering with ionized impurities is $k = k_i = k_f$, but for interband scattering is $k_i \neq k_f$. In Eq. 2.13 the distinction between intra- and interband scattering is made through the factor F :

Chapter 2: Theoretical Background

$m_{hh} = 0.6m_0$	heavy hole mass
$m_{lh} = 0.089m_0$	light hole mass
$\epsilon_S = 12.5$	static dielectric constant
$\epsilon_\infty = 9.61$	high frequency dielectric constant
$\hbar\omega_0 = E_{LO} = 42.6meV$	LO phonon energy

Table 2.1: List of parameters for InP

$$F^{\text{intra}} = \frac{\beta^2 + 2k^2}{k^2} \ln \left(\frac{\beta^2}{\beta^2 + k^2} \right) + \frac{4}{3} \frac{3\beta^4 + 12\beta^2 k^2 + 8k^4}{\beta^2(\beta^2 + 4k^2)}, \quad (2.14)$$

$$F^{\text{inter}} = \frac{\beta^2 + k_i^2 + k_f^2}{k_i k_f} \ln \left(\frac{\beta^2 + (k_i + k_f)^2}{\beta^2 + (k_i - k_f)^2} \right) - 4, \quad (2.15)$$

where $\beta = \sqrt{(N_i e^2 / k_B T \epsilon_0 \epsilon_S)}$ is the inverse screening length. For the calculations a temperature independent density of ionized scatterers $N_i = 10^{24} \text{ m}^{-3}$ was assumed, which means the calculation is most accurate for temperatures above about 70 K (for donor ionization energies of about 6 meV).

The hole scattering mechanism by optical phonons creates or annihilates a phonon with energy $\hbar\omega_0$, therefore the scattering with optical phonons is an inelastic process. The scattering rate for holes by polar optical phonons can be expressed as:

$$P^{\text{Po}} = \frac{e^2 \omega_0 m_f}{4\pi \epsilon_0 \hbar^2} \left(\frac{1}{\epsilon_\infty} - \frac{1}{\epsilon_S} \right) \left\{ \frac{N_0}{N_0 + 1} \right\} \frac{\Psi H}{k_i}, \quad (2.16)$$

where N_0 is the optical phonon occupation number, and the factors N_0 and $N_0 + 1$ refer to absorption and emission of an optical phonon, respectively. Furthermore, $\Psi = \ln |(k_i + k_f)/(k_i - k_f)|$ and the H factors for intra- and interband scattering are:

$$H^{\text{intra}} = [1 + 3\Phi(\Phi - \psi^{-1})]/4, \quad (2.17)$$

$$H^{\text{inter}} = 3[1 - \Phi(\Phi - \psi^{-1})]/4, \quad (2.18)$$

with $\Phi = (k_i^2 + k_f^2)/(2k_i k_f)$.

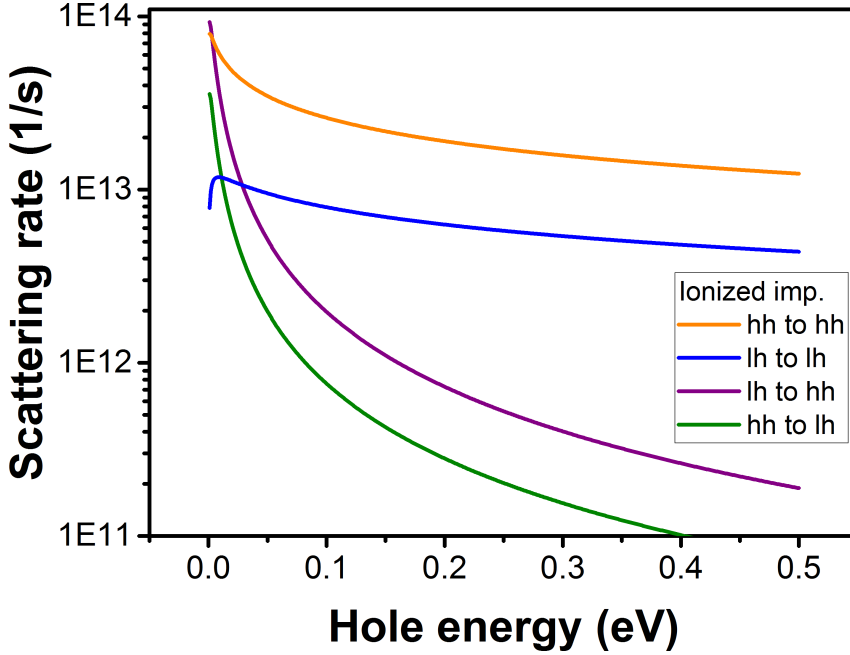


Figure 2.6: Energy dependence of the calculated scattering rates of InP light and heavy holes with ionized impurities at 300 K.

Absorption of photons may excite holes to the heavy hole band, the light hole band and the splitoff hole band. About 20 % of the holes are initially excited to the splitoff band [74] and of the remaining 80 % about one third are excited to the light hole band [75]. A common excitation photon energy for PL measurements is 2.33 eV (532 nm). Absorption of such photons in room temperature InP excites heavy holes about 120 meV below the valence band maximum (VBM), light holes about 470 meV below the VBM and splitoff holes about 370 meV below the VBM (260 meV below the splitoff band maximum).

In InP the spin-orbital splitting energy E_{so} is about 110 meV, which means splitoff holes can only be excited for photon energies higher than $E_g + E_{so}$. For excitation photon energies lower than $E_g + E_{so}$ the absorption excites only light and heavy holes. Most excitation energies used for our upconversion experiments were lower than $E_g + E_{so}$. Absorption of photons with energies

Chapter 2: Theoretical Background

100 meV larger than the bandgap creates in InP heavy holes about 12 meV below the VBM and light holes about 50 meV below the VBM.

The hole energy dependence of the calculated scattering rates of InP light and heavy holes with ionized impurities is shown in Figure 2.6 for 300 K and $N_i = 10^{19} \text{ cm}^{-3}$. The comparison shows that the inter-band scattering rate for scattering from the light hole band to the heavy hole band is stronger than for the reverse scattering process. For hole energies larger than about 5 meV the intraband scattering rates are dominating the scattering with ionized impurities.

Figure 2.7 shows the energy dependence of the InP hole scattering rates with polar optical phonons at room temperature. For comparison, the rates of the inverse scattering mechanisms are shown in the respective graphs. The graphs show that the emission of phonons has the highest scattering rate if it is energetically allowed. For hole energies lower than the optical phonon energy the absorption of phonons dominates. The comparison of the scattering rates with the rates of the reverse scattering mechanism shows that scattering from the light hole band to the heavy hole band is always stronger than the reverse, similar to the results for scattering with ionized impurities (Fig. 2.6).

In doped materials scattering with ionized impurities is an important mechanism, however it does not contribute to hole energy relaxation. For hole energy relaxation, scattering with optical phonons is the most important scattering mechanism [73], whereby phonon emission is dominating for hole energies larger than the optical phonon energies and phonon absorption for lower energies. Scattering with acoustic phonons is the most important hole energy loss mechanism for hole energies lower than the optical phonon energy [73], but has lower scattering rates than the emission of optical phonons if that is energetically allowed. Photo excited holes in the splitoff band relax rapidly by phonon emission into the heavy or light hole band [74] and light holes are quickly scattered into the heavy hole band [75].

Another important scattering mechanism in highly doped material is carrier-carrier scattering. In first approximation the hole-electron scattering could be calculated similar to the scattering with ionized impurities except that the reduced mass of the scattered carriers has to be applied. However, the Pauli exclusion principle has to be taken into account, which means that majority carriers (in n-doped material electrons) have few available final states into which they may scatter. The actual calculation of the scattering rates would require a complicated many-body theory [76].

Important for electron-hole scattering is Rutherford scattering caused by Coulomb interaction, screening of the Coulomb potential for high charge

2.6 Carrier Scattering in Semiconductors

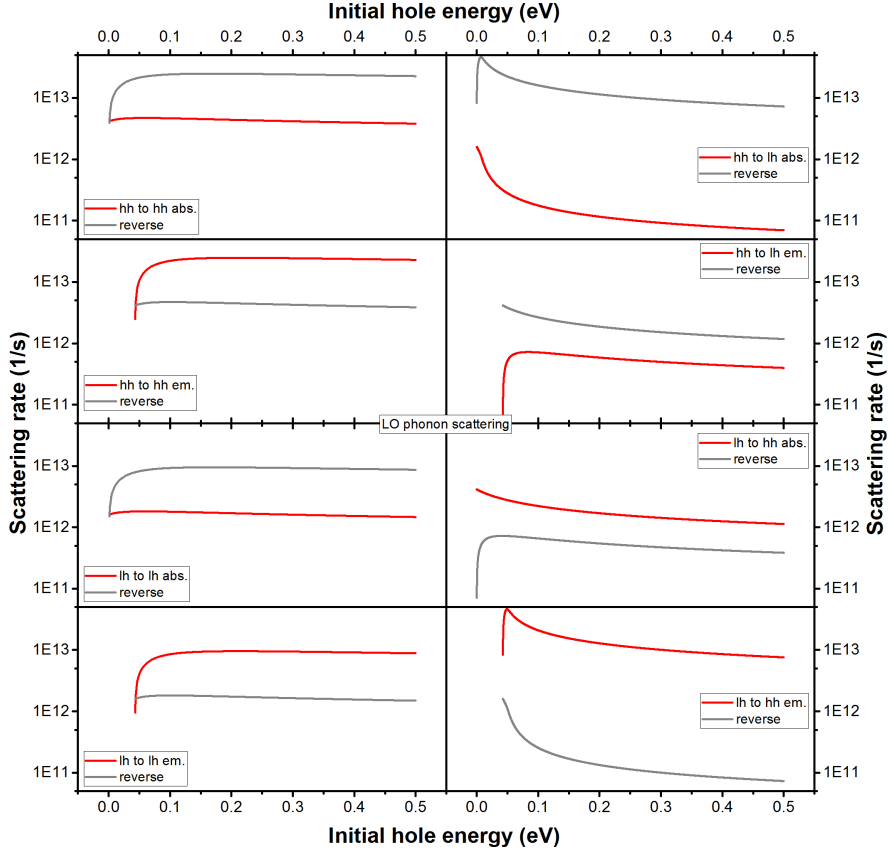


Figure 2.7: Energy dependence of the InP hole scattering rates with LO phonons (absorption and emission) for heavy holes and light holes (red spectra) at 300 K and rates of the respective reverse scattering processes, back to initial hole band, energy, and momentum (grey spectra).

Chapter 2: Theoretical Background

carrier concentrations, and Pauli exclusion principle [77]. Due to energy conservation and Pauli principle the electron-hole scattering rate goes down for $T \rightarrow 0$. The Rutherford scattering rate decreases for increasing temperatures, but The screening effect is enhanced for low temperatures. Thus the theoretical dependence of the electron-hole scattering rate shows the highest scattering rates for temperatures around the Fermi temperature $T_F = \hbar^2/2mk_B(3\pi^2n)^{2/3}$ [78].

Chapter 3

Experimental Details

"...a sophisticated heat beam which we called a 'laser'."

Dr. Evil

3.1 Crystal Growth

The most common semiconducting materials are crystalline solids and it is even possible to find semiconductor crystals in nature as for example pyrite (fool's gold, FeS_2). But, for semiconductor devices very clean and large area crystals are needed. Thus, all semiconductors of industrial importance are artificially produced.

For large scale production the so called Czochralski process [79] is most commonly used. In this process the crystal is grown from a solution only slightly above the melting temperature. A seed crystal is dipped into the solution and then slowly pulled upwards and rotated simultaneously. By precisely controlling the temperature gradients and the pulling and rotation speed, it is possible to extract a large, single-crystalline, cylinder from the melt. The bulk samples studied in Paper IV were grown with the Czochralski process.

The Czochralski process is not suited for nanowire growth or growth of thin films, but epitaxial nanowire growth techniques need a crystalline substrate which is usually fabricated by applying the Czochralski process or a vertical gradient freeze method (VGF). In the VGF method the position of the seed crystal is kept constant and instead the position of the temperature gradient is moved along the growth axis [80].

A method suitable, and widely used, for epitaxial layer growth is growth

from the gas phase also called chemical vapor deposition (CVD) [81]. For CVD the precursor gases are introduced into the growth reactor while the substrate is heated and through chemical reactions a solid layer is deposited on the substrate surface. Low growth pressures are used to reduce parasitic reactions in the gas phase. CVD is applied for the fabrication of high-purity, high-performance solid materials and by the selection of precursor gases the deposited material is determined.

The metallic elements required for compound semiconductors would need very high temperatures to pass into the gaseous phase. One solution to lower the necessary growth temperature, is the employment of metalorganic compounds, which is then called metalorganic vapor phase epitaxy (MOVPE). Typical precursors for the group III elements are trimethyllic or triethyllic compounds whereas usually PH_3 and AsH_3 are used as precursors for phosphorus and arsenic, respectively.

CVD and MOVPE allow a very precise control of doping along the growth direction by simply switching the doping precursor gases. Such doping is called *in situ* doping and has the advantage of not damaging the crystal as much as for example ion implantation.

3.2 Nanowire Growth

The formation of nanowires needs a very anisotropic growth and while some semiconductor materials tend to form nanowires even without catalyst (e.g. ZnO [82]) for most materials a pre-processing of the substrate is required. One of the common ways to initiate nanowire growth is to use gold particles as catalyst [83]. The gold particle determines the position and approximate diameter of the nanowire.

The gold particle acts as a preferential nucleation site for the growth material. If the collected atoms are soluble in the seed particle they are absorbed, which changes the alloy composition in the particle slowly towards supersaturation. As long as the supersaturation in the gas phase is higher than the supersaturation in the particle the precursor atoms will be deposited at the interface to the solid semiconductor material to reach equilibrium. A schematic figure of the wire growth is shown in Figure 3.1. The particle will most likely be liquid during growth and therefore the process is also known as vapor-liquid-solid (VLS) growth mechanism [84].

The gold seed particles can be produced by different methods and each method has advantages and disadvantages. For homogeneous and evenly

3.3 Single Nanowire Measurements

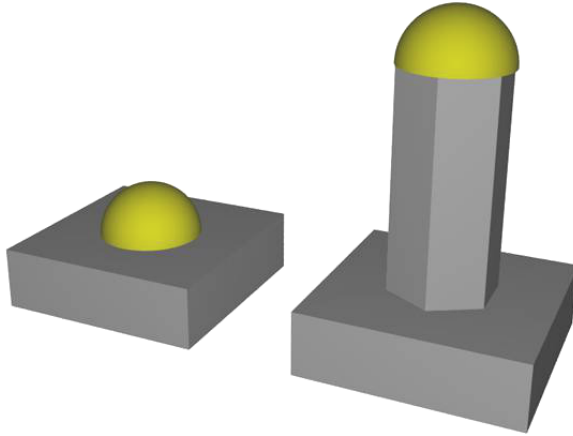


Figure 3.1: Schematic image of the vapor-liquid-solid growth mechanism. To the left the gold particle before nanowire growth and to the right the grown nanowire.

spaced nanowires lithography methods are most eligible, but the process is quite time consuming and expensive. A faster and cheaper method is the fabrication of gold aerosol particles and the deposition of such particles on the growth substrate. The disadvantage of this method is the random positioning on the substrate.

The nanowires studied in Paper I, II and III were grown in a low pressure MOVPE reactor and gold aerosol particles were used as seed particles. The aerosol particles were produced using a spark discharge generator and their size was selected by a set of differential mobility analyzers (DMA). For the growth of InP nanowires the gold aerosol particles were deposited on InP substrates and for the MOVPE growth trimethylindium and PH_3 were used as precursor gases and H_2S as dopant precursor.

3.3 Single Nanowire Measurements

Most semiconductor nanowires are grown homo-epitaxially, which means the substrate is the same material as the nanowires. For optical characterization of the nanowires, such a configuration may cause difficulties, since in first approximation the luminescence intensity scales with sample volume, and



Figure 3.2: Optical microscopy image of nanowires transferred to substrate for optical measurements. The nanowires are about 4 μm long and the substrate is a silicon wafer with patterned gold layer.

thus, the substrate usually outshines the nanowires. For hetero-epitaxially grown wires, i.e. if the substrate material differs from the nanowire material, the nanowire signal can be separated from the substrate luminescence and the measurement is possible.

For photoluminescence measurements on single nanowires the nanowire density on the substrate needs to be low enough to allow a separation of the wires in the optical microscope. The best way to measure individual wire properties is to separate the wires from the growth substrate and deposit them on an optically inactive substrate. The substrates typically used for luminescence measurements are silicon substrates with a thin patterned SiO_2 or gold layer on top. The pattern allows the location and relocation of individual nanowires and thus the study of the same nanowire with various characterization methods.

3.4 Photoluminescence Spectroscopy

Experimentally the transfer is done by touching first the growth substrate and then the silicon substrate with a small piece of cleanroom tissue. Figure 3.2 shows the result of such a nanowire transfer in an optical microscopy image. The nanowires were deposited on a gold layer on a silicon substrate. The laser spot for PL measurements is for the tightest focus of the laser approximately five micrometer in diameter, which means the nanowires must be separated at least that much, which is the case for many of the nanowires seen in the optical microscopy image (Fig. 3.2).

3.4 Photoluminescence Spectroscopy

The term photoluminescence (PL) describes emission of light (luminescence) that is initiated by absorption of photons. As spectroscopic method PL is very sensitive for measuring electronic transitions in the studied material. For PL measurements on semiconducting material typically excitation photon energies much higher than the bandgap of the studied material are used. Absorption of such high energy photons excites electrons from the valence band to the conduction band and thus creates holes in the valence band.

The continuous bands in semiconductors allow nonradiative energy relaxation of the photoexcited electrons and holes to lower band states by emission of phonons. Typically most photoexcited carriers relax to the lowest energy state in the respective band before recombining radiatively. The energy and the intensity of the radiative recombinations are recorded to obtain the PL spectrum of the sample.

The PL spectrum provides information on the energetically lowest radiative states, which in intrinsic and lowly doped semiconductors usually represents the band extrema, excitonic states and defect states close to the badgap. In degenerately doped material the lowest band states are occupied and the radiative recombinations from higher energy states contribute additionally to the PL spectrum.

In practice a PL measurement setup contains many mirrors, filters and lenses, but also other parts are found in almost all PL measurement setups. The most important parts are:

Laser: A stable and powerful light source is required and monochromatic light allows a better separation of luminescence and reflected light.

Optics: to focus the light on the sample and to collect the emitted luminescence.

Chapter 3: Experimental Details

Monochromator: to spatially separate the different photon energies emitted by the sample.

Detector: to record the intensity of the different photon energies emitted by the sample.

Measurements at low temperature require additionally a cryostat to cool the sample to the desired temperature. Typical measurement temperatures are: room temperature (RT), liquid nitrogen temperature (about 77 K), and liquid helium temperature (about 4 K). For spatially resolved PL measurements and measurements on small objects, such as nanowires, some PL setups are equipped with an optical microscope. Such PL measurement setups are called micro PL setups.

The Luminescence setup used for this work was equipped with a continuous flow liquid helium cryostat. In the cryostat the sample was mounted on a cold-finger with help of silver glue to assure a good heat conduction between sample and cold-finger. The sample temperature could be changed by adjusting the the helium flow and by regulating the power dissipation in an electric heater, which allowed PL measurements from liquid helium temperature (4 K) up to 500 K.

Figure 3.3 shows a schematic image of the micro PL setup used in this work. The setup is equipped with two lasers with different optical excitation energies: a frequency doubled solid state laser emitting at 2.33 eV (532 nm) and a tunable pumped Ti:Sapphire laser which enables photon energies from 1.31 eV (945 nm) up to 1.76 eV (705 nm). Both lasers could be focused on the sample from the side by a using lens or from the top by using the microscope objective lens.

The excitation from the side enables a rather homogeneous excitation of an area more than 100 μm in diameter with typical laser power densities about 400 W/cm^2 . The excitation from the top is used for highly focused excitation with laser power densities up to 150 kW/cm^2 . For both excitation paths the excitation power intensity can be controlled by inserting gray filters into the laser beam pass.

To enable a well-defined excitation energy the light emitted by the green, frequency doubled solid state laser, passes a bandpass filter before it is directed to the sample. For the tunable laser instead a computerized monochromator is used as bandpass filter to remove additional laser lines.

In Figure 3.3 the two possible excitation paths are displayed by two different lasers, but both paths are accessible with both lasers. The cryostat with the sample is mounted on a xyz-translation stage to allow focusing of the

3.5 Photoluminescence Excitation Spectroscopy

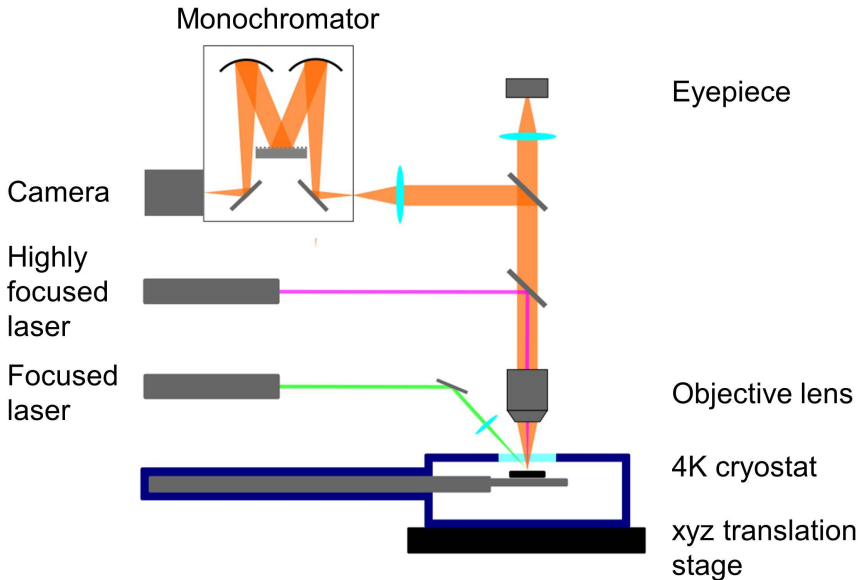


Figure 3.3: Schematic image of a micro PL setup. The laser light can be focused by a lens from the side or through the objective lens. The eyepiece is used to locate the nanowires and the camera detects the luminescence.

microscope and positioning of the field of view precisely on the place or the nanowire of interest. The luminescence from the sample is collected by the microscope objective lens and then directed towards a monochromator, behind which it is recorded by a digital camera.

To avoid damaging of the camera and to prevent scattered laser light from entering the monochromator, a long wavelength edgepass filter is placed at the entrance slit of the monochromator.

3.5 Photoluminescence Excitation Spectroscopy

Photoluminescence excitation spectroscopy (PLE) is an experimental method to probe the absorption to higher excited electron states. The basic principle is exactly the same as in regular PL spectroscopy, but PLE utilizes additionally that the emitted PL intensity depends on the absorption strength of the selected excitation energy.

Chapter 3: Experimental Details

For PLE measurements the luminescence intensity in a selected photon energy interval is detected in dependence of the excitation photon energy. The luminescence is typically detected at energies close to the lowest excited state transition i.e. for semiconductors close to the band gap energy. In intrinsic and lowly doped semiconductors, most of the electrons excited to higher energy states thermalize to the lowest excited state before they recombine. Thus, the detected PLE spectrum contains information about the density of unoccupied states.

In this work for PL measurements and PLE measurement the same setup was used. However, for PLE measurements the long wavelength edgepass filter at the entrance slit of the monochromator had to be replaced. Instead of the edgepass filter two additional monochromators were used acting as a computer controlled band-pass filter which allows measurements very close to the laser wavelength of a tunable laser.

To allow a comparison of the luminescence intensities for different excitation energies, the laser intensity has to be constant for all excitation energies. In our setup that is assured by a computerized feedback loop, which measures the laser intensity and automatically adjusts the optical output power.

3.6 Cross-Polarized Dark Field Spectroscopy

In the previous section I described that two monochromators can be used as computer controlled band-pass filter for luminescence measurements close to the laser line. Another method for measurements very close to the laser energy is cross-polarized dark field PL. In this method the excitation light polarization is orthogonal to the detection polarization [85].

The setup used in this work is depicted schematically in Figure 3.4. The combination of polarizing beam splitters, achromatic lenses and pinhole, lower the detected laser intensity up to five orders of magnitude. The strong suppression of laser intensity entering the monochromator, allows a simultaneous measurement of the luminescence on both sides of the laser although the laser energy is detected in the same energy range.

To allow the application of the cross-polarized dark field method for PLE measurements, the excitation laser intensity is measured by a power meter and the laser intensity is automatically adjusted over the whole range of available laser wavelengths. Cross-polarized dark field PLE enables the simultaneous measurement of upconversion and downconversion PL and PLE.

3.6 Cross-Polarized Dark Field Spectroscopy

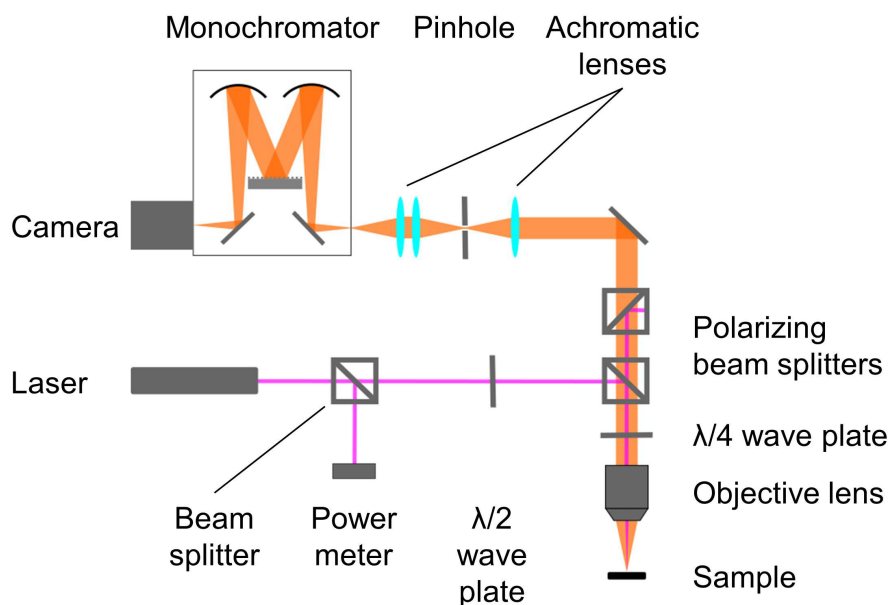


Figure 3.4: Schematic image of the cross-polarized dark field PL setup. The $\lambda/2$ wave plate is used to adjust the laser light polarization to the alignment of the polarizing beam splitter cubes. The combination of polarizing beam splitters, achromatic lenses and pinhole strongly suppresses the laser light intensity in the monochromator and the camera.

Chapter 4

Results

“Oh, figures!” answered Ned. ‘You can make figures do whatever you want.’”

Jules Verne in “20,000 Leagues Under The Sea”

In this chapter I will summarize some of the findings of the papers attached to the thesis and present some further supplementing experimental results.

4.1 Probing the Conduction Band Structure

Doping is necessary for most electronic device applications to control the conductivity of the semiconducting material. In nanowires the incorporation of doping atoms may furthermore have a quite strong effect on the growth mechanism [86–88], which may change the shape, the growth rate and the crystal structure of the nanowires. For Paper I, we studied the effect of sulfur doping of InP nanowires and observed that the n-dopant induces perfect wurtzite crystal structure.

The nanowires for this study were grown from deposited 80 nm gold aerosol particles in a 100 mbar low-pressure MOVPE system and H₂S was used as dopant. The addition of H₂S did not only dope the material, but also strongly increased the axial growth rate and decreased the radial growth rate. The increase of the axial growth rate can be explained by the exponential dependence of the growth rate on the steady-state supersaturation and the radial growth rate may be due to a smoother surface of the wurtzite crystal structure with fewer nucleation sites.

Figure 4.1 shows high-resolution transmission electron microscopy (TEM) images, scanning electron microscopy (SEM) images and the dependence of

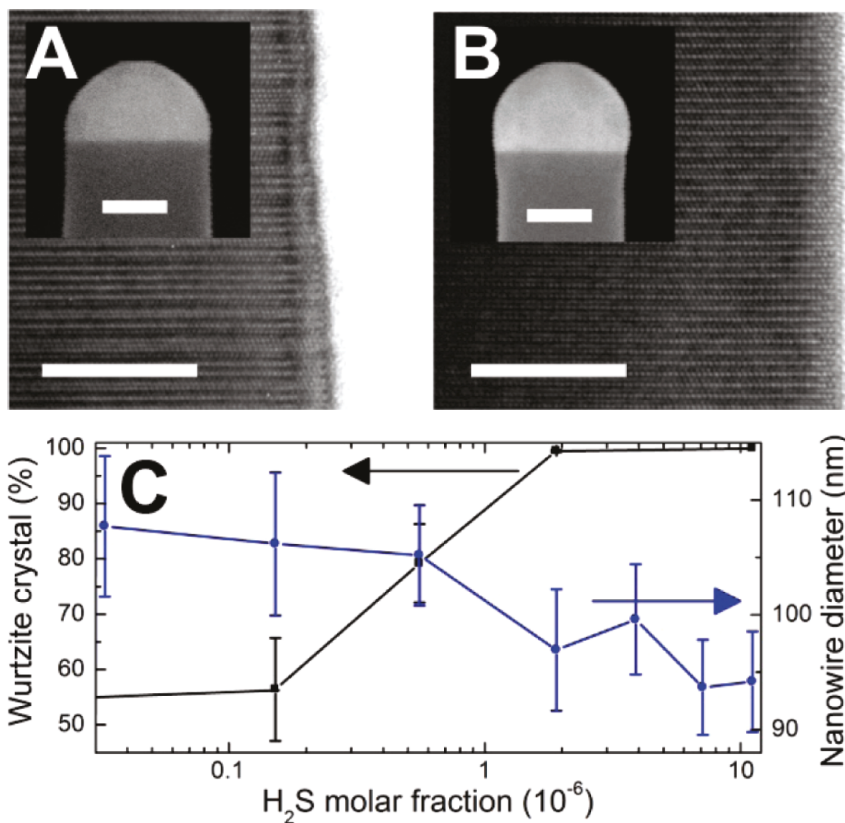


Figure 4.1: (A) and (B) are high-resolution TEM images of InP nanowires grown with $\chi_{H_2S} = 0$ and $\chi_{H_2S} = 11.1 \times 10^{-6}$, respectively the scale bars are 10 nm. The insets show SEM images of the same sample with 50 nm scale bar. (C) Wurtzite crystal structure, as percent of total, and nanowire diameter, versus H₂S molar fraction during growth.

4.1 Probing the Conduction Band Structure

the relative amount of wurtzite in the nanowires and the nanowire diameter on the H_2S precursor concentration. The TEM analysis shows that the undoped reference nanowires have a mixed crystal structure with approximately the same amount of zincblende as wurtzite. With increasing doping concentration the amount of wurtzite increases and for the highest H_2S concentration only one stacking fault was found in a total of five investigated nanowires.

InP layers and InP bulk material typically crystallize in the zincblende phase and the properties of this phase are well known (e.g. [89] and the references therein). The wurtzite phase of InP on the other hand is a very new material and the physical properties are still investigated. De and Pryor computed the band structure of InP using an empirical pseudopotential method and predicted that wurtzite InP should have an unusual conduction band structure with a second minimum at the gamma point only 0.24 eV above the first minimum [90].

Experimentally the predictions about the semiconductor band structure close to the Γ -point can be tested by applying luminescence measurements. The band gap and the valence band splitting energy of wurtzite InP were, for example, measured using photoluminescence and photoluminescence excitation spectroscopy [91, 92].

For Paper I, we took advantage of the strong state-filling in highly doped semiconductors, to probe the conduction bands and experimentally verify the predicted second conduction band minimum. The typical photoluminescence spectra for undoped nanowires and nanowires with increasing doping concentrations are shown in Figure 4.2. The undoped reference nanowires exhibit a mixed crystal structure with a luminescence peak for photon energies around 1.45 eV. Such luminescence lies energetically between the band-gap energies of zincblende InP (1.424 eV at 4 K [93]) and wurtzite InP (about 1.49 eV at 4 K [92, 94, 95]), which is typical for mixed crystal structure InP nanowires [96]. With increasing doping concentrations the Burstein-Moss effect shifts the luminescence edge to higher energies and the band gap renormalization effects extend the luminescence to lower energies.

The Burstein-Moss shift can be used to calculate the carrier concentration from the luminescence data as described in Chapter 2.2. By using the theoretically predicted carrier masses [90] and parabolic bands for the calculation, the electron density is estimated to be $3.4 \times 10^{18} \text{ cm}^{-3}$ for a H_2S precursor molar fraction of 1.9×10^{-6} . From energy-dispersive x-ray spectroscopy (EDX) the determined sulfur concentration was $1.3 \times 10^{20} \text{ cm}^{-3}$.

One reason for the different doping concentrations determined by PL and

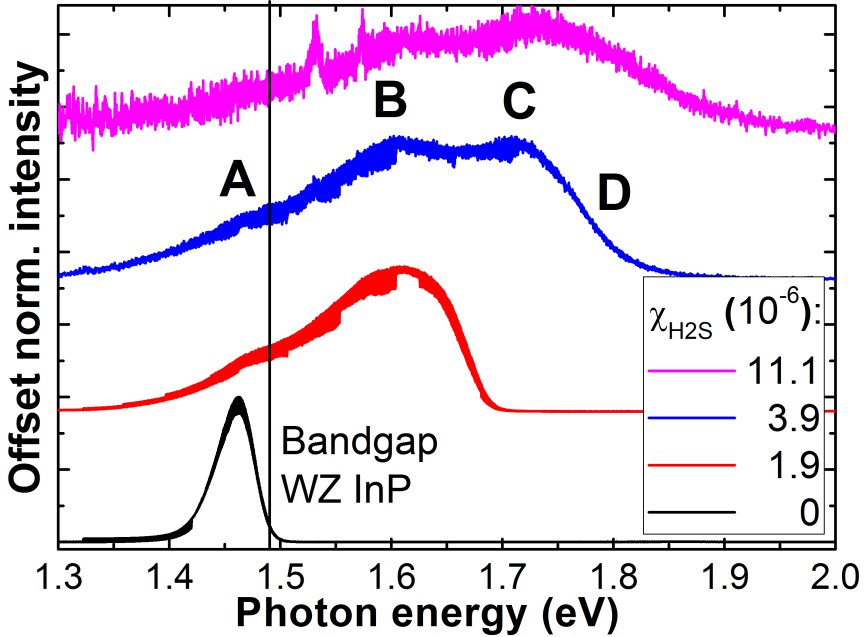


Figure 4.2: PL of single nanowires grown with varying H_2S molar fractions. The bandgap of wurtzite InP is indicated by the vertical black line. The cryostat temperature was 4 K.

EDX measurements, may be the uncertainty of the charge carrier masses in wurtzite InP and the assumption of isotropic parabolic bands without \mathbf{k} -dispersion for the calculation of the Burstein-Moss shift. A second reason is the systematic difference between the methods. EDX measures the chemical composition and PL measurements the charge carrier concentration and many sulfur atoms may not act as donors. The EDX measurement results indicate that the surface of the highly doped nanowires may be passivated by sulfur atoms and such a passivation would give rise to approximately the observed difference between sulfur concentration and doping concentration.

The PL spectra of the highest doped samples shown in Figure 4.2 exhibit not only a weak shoulder around the wurtzite InP band gap (marked as A in the figure), but also a second peak around 1.73 eV (marked as C in the figure). The spectral shape of the Burstein-Moss shifted luminescence reflects the transition probability as well as the density of states in the conduction

4.1 Probing the Conduction Band Structure

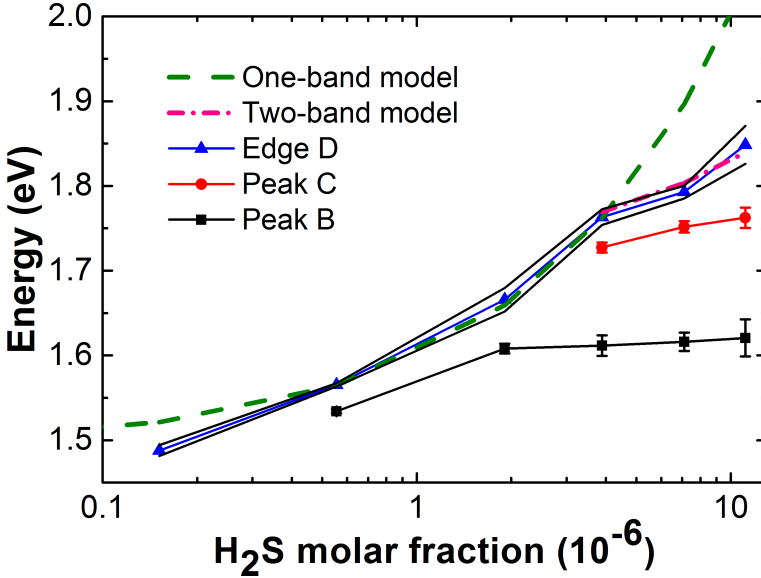


Figure 4.3: Dependence of spectral features seen in Figure 4.2 on the molar fraction of H₂S. For high H₂S molar fractions the dependence diverges from the one-band model.

band, and a single conduction band should not give rise to a distinct additional peak. The two quite closely separated valence bands which have been observed using PLE [94, 95] are improbable origins, because the peak is only seen for high doping concentrations and the relative peak intensity does not depend on the excitation intensity. Thus, the high-energy peak, C, in our PL spectra is most likely the predicted second gamma point [90], and we interpret the PL for very high doping concentrations as radiative recombination from two conduction bands.

The dependence of the spectral features on the doping concentration presented in Figure 4.3 supports the second conduction band model. In a one-band model of the state filling, the energy shift for the high doping concentrations should be stronger than observed, whereas the dependence fits well with a two-band state filling model. The equation for the displayed one-band model is $E = 1.49 + 1100\chi_{H_2S}^{2/3}$ (eV), and the equation for the two-band model is $E = 1.70 + 280\chi_{H_2S}^{2/3}$ (eV).

4.2 Electron Gas Temperature

For Paper II, we studied more detailed the PL spectra of degenerately doped InP nanowires with Burstein-Moss shift less than the energy separation between the two conduction bands. Figure 4.4 shows a comparison of the doping concentration dependence of the PL spectra and the PLE spectra of the same samples. The Burstein-Moss state-filling is visible in the PL spectra as extension of the PL spectra to higher photon energies and in the PLE spectra as a shift of the steep on-set to higher energies. Such a shift of the absorption edge is expected from the state filling of the conduction band states (see Chapter 2.2). At 4 K measurement temperature, 5 meV below the Fermi energy, less than 10^{-6} states are unoccupied and noticeable absorption should start approximately $4 k_B T$ (1.4 meV at 4 K) below the Fermi energy. However, in the PLE spectrum of sample IV in Figure 4.4, significant absorption can be seen already for much lower photon energies starting at about 1.5 eV.

Some possible mechanisms for photon absorption with energies much lower than the Fermi energy are: phonon assisted indirect absorption, intra-valence band absorption, free carrier absorption, and two-photon absorption. However, in PLE measurements absorption is only detected if it is followed by radiative recombination. Intra-valence band absorption and free carrier absorption usually do not cause luminescence and do not contribute to an increase of the PLE signal. Phonon assisted indirect absorption enables radiative recombination, but it would lower the absorption edge only about the energy of the involved phonon. Two-photon absorption can also result in radiative recombination, but it requires very high excitation intensities and absorption would start already below the bandgap energy.

Single photon direct band-to-band absorption requires unoccupied conduction band states. An elevated electron gas temperature would imply unoccupied states below the Fermi energy (see Chapter 2.3), but to explain the observed absorption far below the Fermi energy, the electron gas temperature has to be much higher than the 4 K cryostat temperature. To estimate the actual electron gas temperature in the samples we analyzed the spectral PL shape.

If an even hole distribution is assumed, the spectral line shape of \mathbf{k} -conserving band-to-band recombinations is proportional to the product of the density of states and the Fermi-Dirac distribution function [20]. The Fermi-Dirac distribution is directly temperature dependent, and thus, the electron gas temperature of a degenerately doped semiconductor can be estimated from the line shape of the PL spectra. To calculate the electron temperature

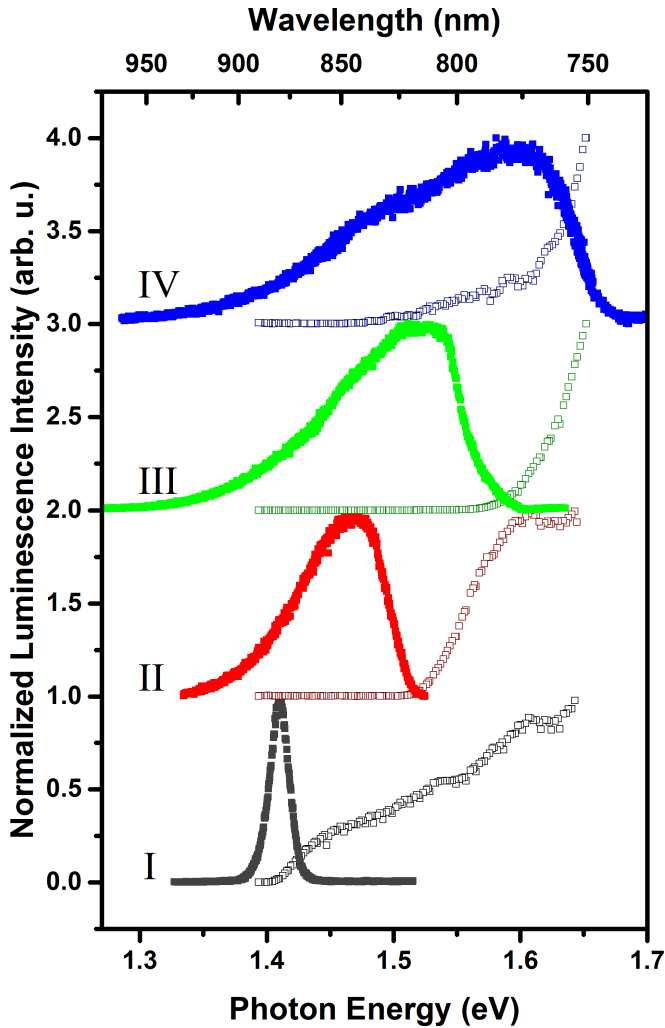


Figure 4.4: Low temperature PL (filled squares) and PLE spectra (hollow squares) of individual nanowires normalized to the same maximum intensity. (I) A nominally undoped nanowire and from (II) to (IV) nanowires with increasing doping concentration. The doping concentration of spectrum IV is comparable to the the doping for the red spectrum in Figure 4.2. The detection energy for the PLE was at 1.38 eV.

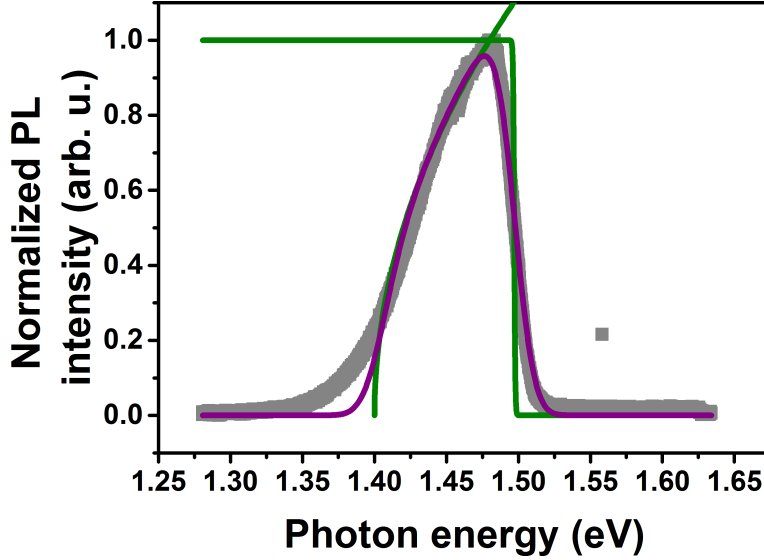


Figure 4.5: The best fit of an n-doped InP nanowire PL spectrum measured at 4 K. The parabolic density of states and the Fermi-Dirac distribution are shown together with the resulting function after convolution with a Gaussian peak.

we assume isotropic, parabolic bands with a density of states

$$I_{\text{DOS}}(E) = \sqrt{\frac{E - E_g}{E_m}}, \quad (4.1)$$

and filling of the conduction band states according to the Fermi-Dirac distribution

$$I_{\text{Fermi}} = \frac{1}{1 + \exp \frac{E - E_F}{k_B T}}. \quad (4.2)$$

Where E_g is the bandgap, $E_m \propto \pi^4 \hbar^6 / 2m^3$ was used as fitting parameter for the effective mass m , E_F is the Fermi energy, k_B is the Boltzmann constant and T the absolute temperature. The product of Eq. 4.1 and Eq. 4.2 was convoluted with a Gaussian peak to account for intrinsic broadening effects. The resulting fitting functions are shown in Figure 4.5 together with a

4.2 Electron Gas Temperature

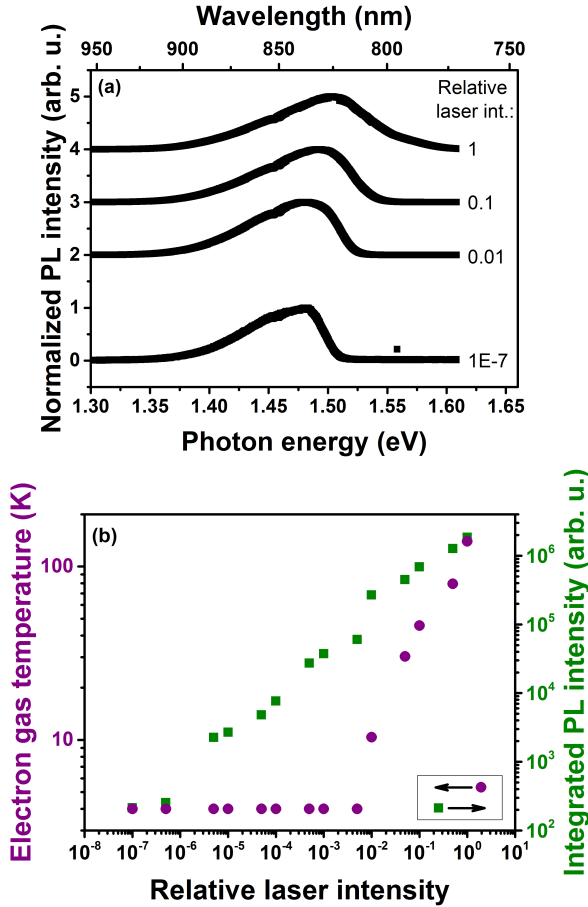


Figure 4.6: Laser intensity dependence of n-doped InP nanowires at a cryostat temperature of 4 K: (a) Normalized PL spectra with increasing laser intensity from bottom to top ($\lambda = 750$ nm, 1.65 eV). (b) Integrated PL intensity and electron temperature. The latter was calculated from PL spectra using a parabolic density of states multiplied by a Fermi-Dirac distribution and convoluted by a Gaussian broadening peak as fitting function. 4 K was set as lower temperature limit. The width of the Gaussian broadening was assumed to be a sample specific constant, which was fitted for the lowest laser intensity and then kept constant for the other laser intensities.

Chapter 4: Results

PL spectrum measured at 4 K and at low excitation intensity. The cryostat temperature (4 K) was set as lower limit for the temperature variable T .

The influence of the laser intensity on the electron gas temperature is visible in Figure 4.6. Figure 4.6 (a) shows PL spectra for different laser intensities and (b) the estimated electron gas temperature and the integrated PL intensity. For low laser intensities the calculated electron gas temperature is equal to the cryostat temperature, but for laser intensities of at least 1 % of the full laser intensity, the electron gas temperature increases drastically with increasing laser intensity. The direct dependence of the electron gas temperature on the laser intensity shows that at high laser intensities the laser heats the electron gas.

The laser intensity dependence of the integrated PL intensity (Fig. 4.6 (b)) exhibits a power law dependence ($I \propto P^\alpha$) with exponent $\alpha < 1$. As described in Chapter 2.4, the exponent of the power law dependence contains information about the dominating absorption-recombination processes and $\alpha < 1$ is usually attributed to Auger generation-recombination processes. Thus, the electron gas heating process is probably driven by Auger processes.

J. Shah reported that intense photoexcitation can create a hot electron gas in semiconductors and that the electron gas acquires energy from the photoexcited electrons [97], but very high laser powers were needed to observe the electron heating. J. Shah studied GaAs and measured, for example, electron temperatures around 76 K with a laser intensity of 100 kW/cm². The sample was kept at 2 K and the rise in lattice temperature was insignificant. The reasons for the much higher electron temperature in the samples studied in this work at laser intensities below 400 W/cm² are most likely the small nanowire dimension and the high doping concentration. With laser spot sizes larger than the studied nanowires the whole nanowire is heated and the high doping concentration strongly increases carrier-carrier scattering [97].

Figure 4.7 shows another indication for heating of the conduction band electrons in our measurements. The figure shows the luminescence of a single nanowire for continuous excitation and for pulsed laser excitation. For the continuous excitation measurement, the laser intensity was lowered with a gray filter to 8 % of the total laser intensity and for the pulsed excitation measurement a chopper was used, which reduced the integrated laser intensity about the same amount. The total energy transfer was the same for both excitation methods, but the two spectra exhibit a significant difference.

By fitting the high-energy side of the spectra with a Fermi-Dirac distribution, the Fermi energy and the electron gas temperature for the two excita-

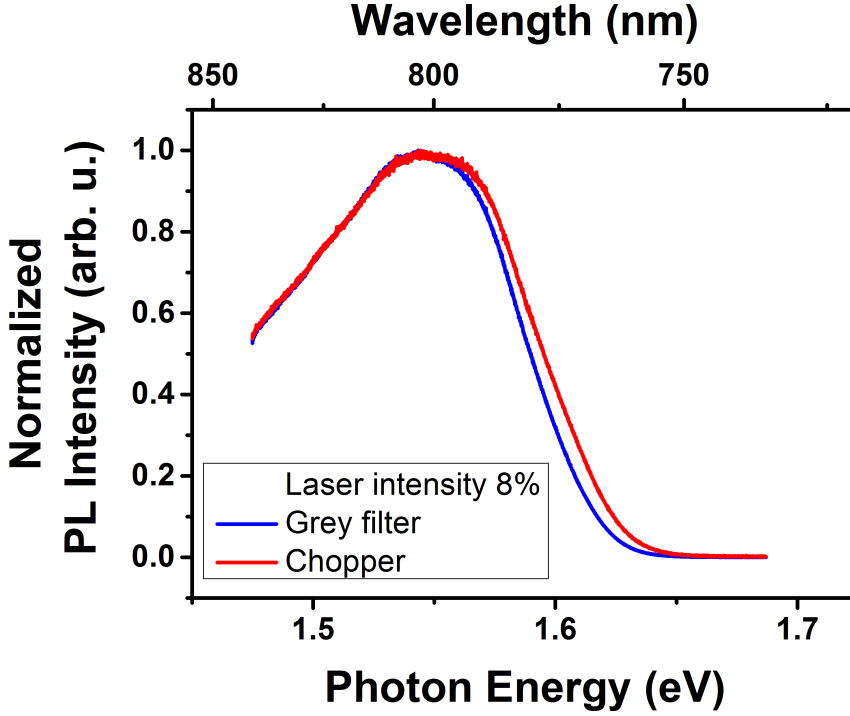


Figure 4.7: Normalized PL spectra of a single nanowire excited by a 532 nm continuous wave laser (gray filter) and pulsed laser light (chopper) with the same integrated intensity measured at 4 K cryostat temperature.

	Max. PL Int.	E_F in eV	T_F in K
Grey filter	303137	1.590	144
Chopper	52012	1.595	155

Table 4.1: Maximum PL intensity, Fermi energy and electron temperature calculated from the continuous wave and the pulsed laser illumination spectra shown in Figure 4.7.

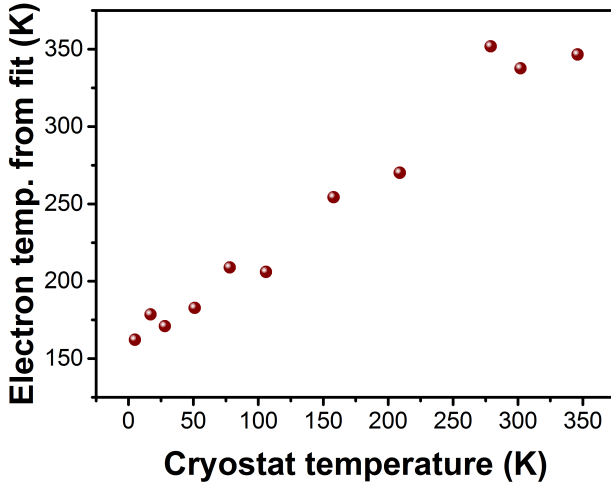


Figure 4.8: Cryostat temperature dependence of the electron gas temperature in n-doped InP nanowires, estimated through a fitting procedure of the PL spectra assuming a Fermi-Dirac distribution of the conduction band electrons in a parabolic isotropic conduction band.

tion conditions were estimated. The resulting parameters are summarized in Table 4.1. For continuous wave excitation the estimated electron gas temperature is 144 K. When the chopper is used the illumination is a short intense laser pulse and due to the short electron life time, the luminescence represents a snap shot of the electron temperature during and short after the excitation. The estimated electron gas temperature for pulsed excitation is 155 K while the Fermi energy changes only marginally from 1.590 eV for continuous wave excitation to 1.595 eV for pulsed laser excitation.

For the estimation of the electron gas temperature we used a very simplified fitting procedure and neglected band structure, intrinsic broadening and inhomogeneous hole distributions. However, the different excitation conditions should not change the physical properties of the sample and the results indicate a significant, but rather low, increase of the electron gas temperature for pulsed excitation, compared to continuous wave excitation. For pulsed excitation, the instantaneous power was about 12 times higher (during the laser pulse) than the power for continuous wave excitation, but the PL in-

tensity was about five-times lower for pulsed excitation. Together with the calculated higher electron gas temperature for pulsed excitation, this indicates that the electron gas cools to a lower temperature between the pulses.

For electrons far above the Fermi energy the dominating scattering mechanisms are scattering with polar optical phonons and with other conduction band electrons [97]. At high temperature the scattering with optical phonons is faster and at low temperature the electron-electron scattering dominates [98]. Thus, at high system temperatures the electron gas heating effect of photo-excited electrons is lower than for low system temperatures. This effect is seen in Figure 4.8, where the cryostat temperature dependence of the calculated electron gas temperature is depicted. At low cryostat temperatures the calculated electron temperature is more than 150 K higher than the measured cryostat temperature, but at room temperature and above, at identical laser intensities, the heating effect is almost negligible. At low temperature the excess energy is transferred to the electron gas and at high temperature it is transferred to the LO-phonon system [99].

4.3 Photon Downconversion

In the previous section, I showed that photoexcitation with a laser may heat the conduction band electron gas in degenerately doped semiconductors and that the elevated electron gas temperature may allow band-to-band absorption with photon energies far below the Fermi energy. Such absorption was visible as luminescence in the PLE spectra in Figure 4.4. For those PLE measurements the laser excitation energy was higher than the energy of detection and the same is true for the PL spectra in the previous sections. Such luminescence with photon energies lower than the exciting laser is called downconversion PL.

In this section, I will discuss photon downconversion PL for excitation close to the Fermi energy and below and compare the results for n-doped InP nanowires (published in Paper II) with results of similar measurements on n-doped bulk InP (part of Paper IV).

Figure 4.9 shows the excitation energy dependence of the InP nanowire luminescence measured at 4 K cryostat temperature. Figure 4.10 shows the results of similar measurements on n-doped bulk InP for 4 K (Fig. 4.10 (a)) and 100 K (Fig. 4.10 (b)) cryostat temperature. In the measurements on nanowires we observed luminescence (and thus absorption) for all selected excitation energies higher than the bandgap of InP. For bulk InP at 4 K the PL

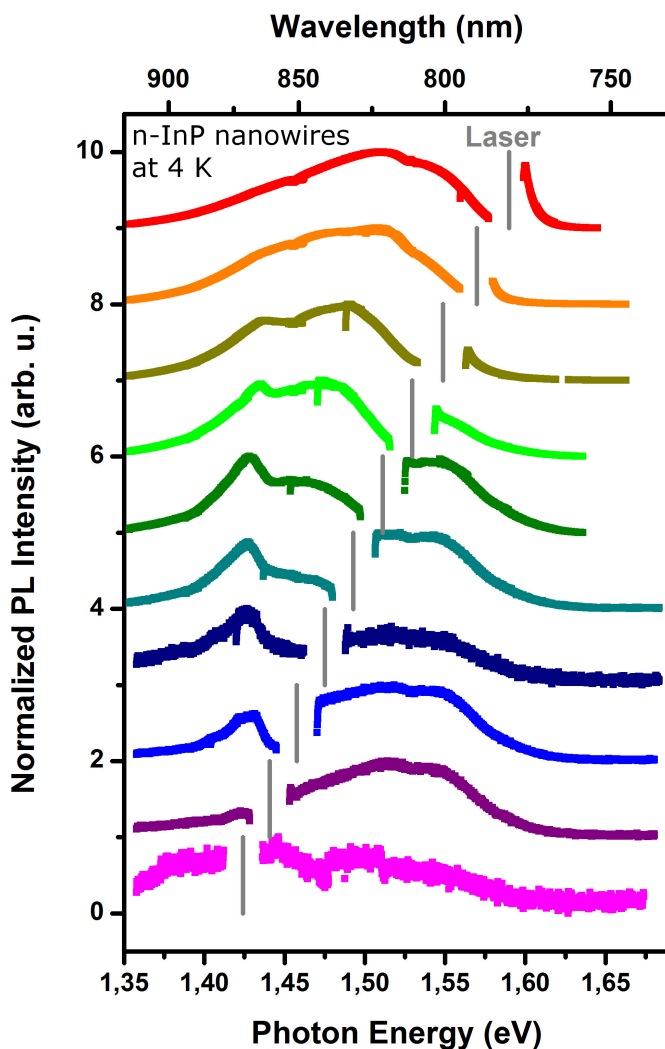


Figure 4.9: Normalized PL spectra for a highly n-doped nanowire sample (corresponding to spectrum III in Fig. 4.4) for different energies of the exciting laser. The gray vertical lines indicate the exciting laser energy. The integration time above the laser energy was 20 times higher than below the laser energy. The cryostat temperature was 4 K.

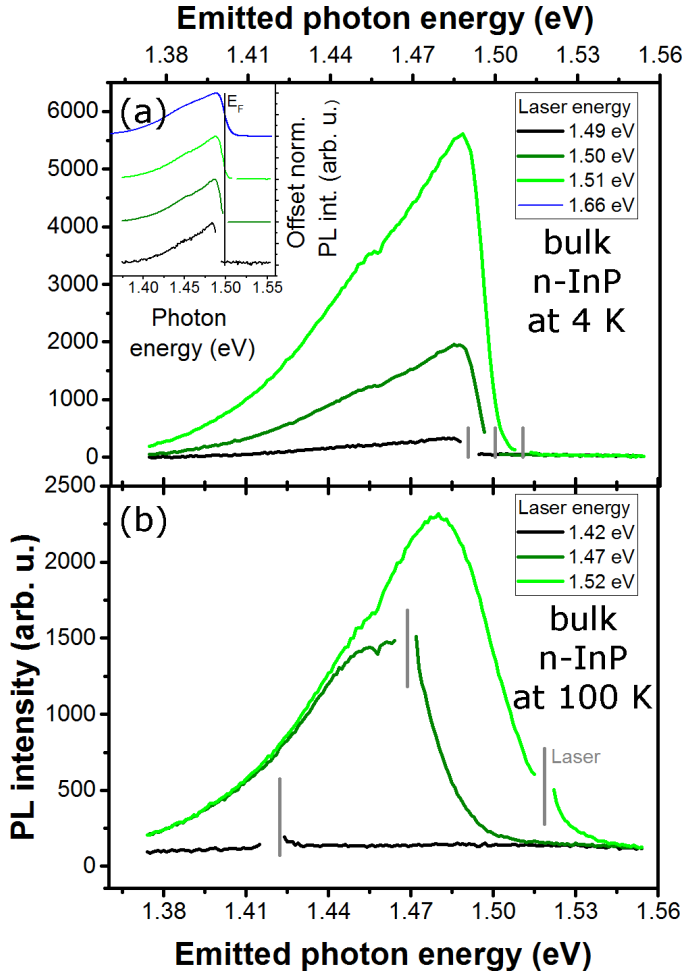


Figure 4.10: PL spectra of n-doped bulk InP samples for selected excitation energies measured at 4 K (a) and at 100 K (b). The excitation laser energy is indicated by vertical gray lines. Inset in (a): Normalized PL spectra including low excitation intensity PL for 2.33 eV excitation. The vertical black line indicates the doping induced Fermi energy estimated from the PL spectrum for 2.33 eV excitation.

Chapter 4: Results

signal intensity dropped below the noise level for excitation energies lower than 1.49 eV. For measurements at 100 K we could observe luminescence further below the Fermi energy, but still not for energies as low as for the measurements on nanowires.

The comparison of the luminescence results for measurements on nanowires and on bulk InP, indicates that the laser induced heating effect is stronger in nanowires. A possible explanation for the more efficient heating of nanowires could be the small size of the nanowires in comparison to the excitation laser spot size on the sample. Thus, in PL measurements on nanowires the whole nanowire is optically pumped, while in bulk material the pumped electron gas is surrounded by colder electrons outside of the excitation volume.

In degenerately n-doped semiconductors the absorption of photons with energies lower than the Fermi energy is limited by the number of available conduction band states. However, the radiative recombination is limited by number and properties of the photogenerated holes. In scientific literature the radiative recombination process in degenerately n-doped semiconductors, is commonly described by fast relaxation of the photoexcited hole to the valence band maximum or to acceptor states, which is then followed by recombination with a conduction band electron at any position in k -space (see for example [27–30]). It is claimed that the \mathbf{k} -conservation rule is abrogated in degenerately doped semiconductors due to localization of the acceptor states in real space [28] or by carrier scattering with ionized impurities [27].

A dominantly non- \mathbf{k} -conserving recombination process would mean that the spectral PL shape is independent of the \mathbf{k} -vector of the photoexcited hole, and thus, independent of the energy of the absorbed photon. However, our PL measurement results for n-doped bulk InP show a spectral change with changing excitation energy. The spectral difference is most pronounced at 100 K measurement temperature, in a comparison of excitation at 1.47 eV with excitation at 1.52 eV (Fig. 4.10 (b)). Due to the spectral difference, we exclude an exclusively non- \mathbf{k} -conserving recombination process. Instead we suppose that most photoexcited holes recombine radiatively with conduction band electrons before reaching the valence band maximum and that the dominant radiative recombination mechanism is \mathbf{k} -conserving recombination of hot holes with conduction band electrons with similar \mathbf{k} .

A comparison of the PL spectra of n-doped InP nanowires (Fig. 4.9) seems to support the conclusions we draw from the bulk spectra. However, the most interesting feature of the spectra in Figure 4.9 is the observed luminescence at energies higher than the laser photon energy, the upconversion PL.

4.4 Photon Upconversion in n-doped InP

The 4 K nanowire PL spectra in Figure 4.9 and also the 100 K PL spectra of n-doped bulk InP (Fig. 4.10 (b)) show luminescence on both sides of the laser energy; downconversion PL below the laser energy and upconversion PL above. The mechanism resulting in upconversion will be discussed in this section.

Absorption of a photon creates a hole with a specific \mathbf{k} -vector, \mathbf{k}_{ex} , typically with $k_{\text{ex}} > 0$. Scattering of the photoexcited hole, in most cases, leads to energy and momentum relaxation, which causes a reduction of the k -value of the hole. Direct, \mathbf{k} -conserving transitions of conduction band electrons with holes at $k < k_{\text{ex}}$ are visible as photon downconversion in PL measurements, as discussed in the previous section.

Photon upconversion requires either holes at $k > k_{\text{ex}}$ or \mathbf{k} -indirect transitions. In Paper II we argued that \mathbf{k} -indirect recombinations could cause the photon upconversion. However, after further measurements (condensed in Paper III and IV) we now argue that even the upconversion PL is dominated by \mathbf{k} -conserving direct recombinations.

The temperature dependence of the upconversion intensity, which is shown in Figure 4.11 for n-doped InP nanowires, provides a first indication that \mathbf{k} -indirect recombination is not the main reason for the observed upconversion. The upconversion intensity relative to the downconversion intensity decreases strongly with decreasing temperature. Which is in contrast to the luminescence intensity dependence in crystalline silicon, where the radiative recombination coefficient increases with decreasing temperature [100] and in crystalline silicon the radiative recombination is completely dominated by \mathbf{k} -indirect phonon assisted recombinations.

The measurements on n-doped bulk InP show a temperature dependence of the upconversion similar to the upconversion in nanowires. Figure 4.10 shows the photon upconversion and downconversion PL of n-doped bulk InP for 4 K and 100 K cryostat temperature. At 4 K the upconversion intensity vanished completely. Even more interesting is the change of the upconversion PL for different excitation energies at 100 K. For \mathbf{k} -indirect recombinations the spectral shape of the upconversion PL should not depend on the excitation energy or the \mathbf{k} -vector of the photoexcited hole. The optical phonon assisted recombination would not suppress recombinations with electrons at high k .

As possible upconversion mechanism, instead of \mathbf{k} -indirect recombinations, we propose that photon upconversion in degenerately n-doped di-

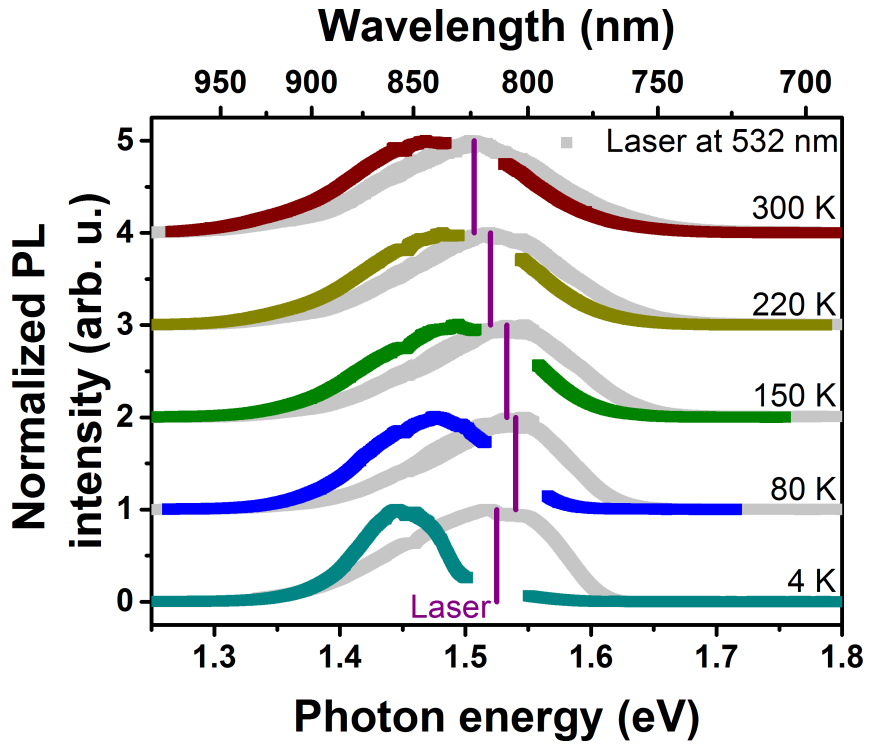


Figure 4.11: Temperature dependence of n-doped InP nanowire PL spectra for 2.33 eV excitation (gray spectra) and excitation at the PL peak maximum (colored spectra). The laser photon energy is indicated by the vertical purple lines.

4.4 Photon Upconversion in *n*-doped InP

rect band semiconductors is caused by scattering of valence band holes to higher k -values followed by \mathbf{k} -direct recombinations with conduction band electrons at similar \mathbf{k} . The temperature dependence of such upconversion is then determined by the temperature dependence of the k -increasing scattering mechanism.

One possible scattering process to higher k -values involves the absorption of optical phonons. Scattering with optical phonons changes not only the \mathbf{k} -vector of the hole, but also increases (or decreases, for phonon emission) the energy of the scattering hole about the optical phonon energy. Figure 4.12 shows the possible scattering processes for photoexcited light and heavy holes with LO phonons.

Most of the photoexcited light holes will scatter to the heavy hole band (see Chapter 2.6) and cause photon downconversion with a low energy shift or heavy holes with k much larger than k_F . For the shown photon energy (100 meV higher than the bandgap, similar to the experimental conditions for Fig. 4.11) heavy holes are created less than the LO phonon energy below the valence band maximum, which means that for heavy holes emission of phonons is prohibited and phonon absorption is the only allowed optical phonon scattering process and scattering within the heavy hole band has a higher probability than scattering to the light hole band (see Chapter 2.6).

Optical phonon scattering of photoexcited heavy and light holes both display scattering to k -values higher than k_F and momentum relaxation of such high- k holes allows \mathbf{k} -conserving direct recombinations with energies higher than the energy of the absorbed laser photon.

Scattering with optical phonons is only one possible scattering mechanisms that can cause scattering of holes to higher k -values, but the spectral shape of downconversion in Figure 4.11 indicates that (at least in nanowires) the scattering with optical phonons contributes strongly to the momentum distribution of holes. The spectra in Figure 4.11 show a decrease in intensity for photon energies right below the laser energy which could be attributed to an discrete energy jump of the photoexcited holes to lower k -values. The most likely candidate for such a scattering event is emission of an optical phonon.

Figure 4.13 (a) to (c) show the excitation energy dependence of the normalized luminescence of *n*-doped InP bulk samples. A horizontal cut line through the contour plot corresponds to a PL spectrum with excitation energy determined by the vertical coordinate. A selection of such horizontal cut lines through the non-normalized contour plots has already been presented in Figure 4.10. The excitation energy is in Figure 4.13 visible as diagonal

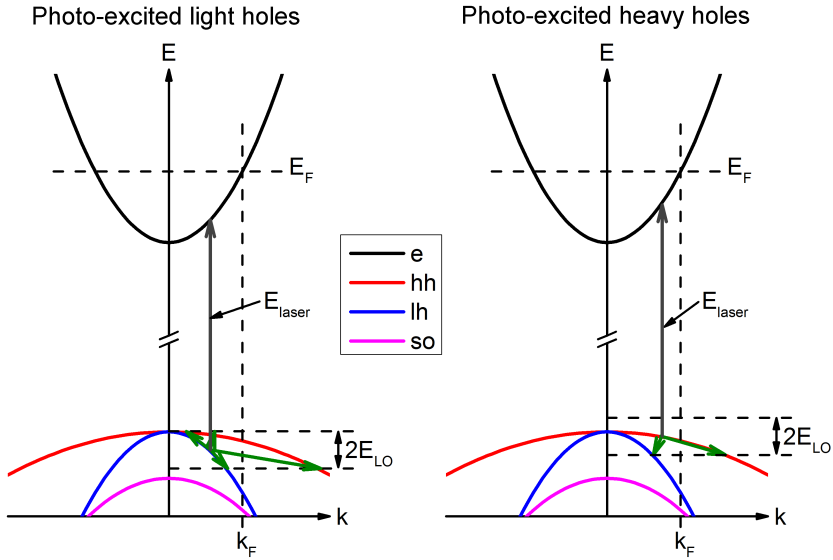


Figure 4.12: Illustration of different scattering paths involving optical phonons. The figure is to scale (effective masses and band edge energies for zincblende InP were used), apart from the bandgap which has been decreased for clarity. The absorbed photon energy is 100 meV higher than the bandgap and the optical phonon energy was taken to be 42.6 meV, which corresponds to the LO phonon energy. We neglect the k dependence of the LO phonon energy and the carrier masses. Left panel: If holes are created in the light hole band, they may scatter to lower energy by emission of an optical phonon causing downconverted luminescence. Absorption of an optical phonon causes scattering to the light hole band or to the heavy hole band and both can be seen as photon upconversion, but only scattering to the heavy hole band enables photon emission at energies much higher than the absorbed photon. Right panel: Illustration of holes created in the heavy hole band, where (for the shown excitation energy) scattering by optical phonons can only cause photon upconversion.

4.4 Photon Upconversion in n-doped InP

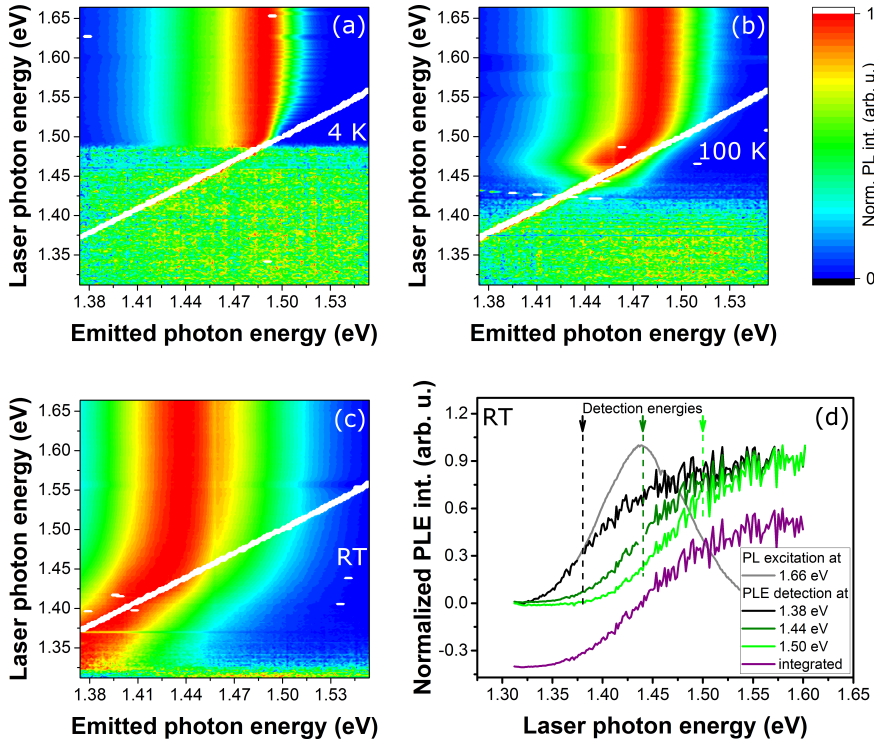


Figure 4.13: Excitation energy dependence of the normalized luminescence of n-doped InP bulk samples as photon energy contour plots measured at 4 K (a), 100 K (b) and at room temperature (c). (d) Normalized room temperature PLE spectra for selected detection energies and integrated PLE intensity. The detection energy is indicated by arrows and vertical dashed lines. The gray spectrum shows the room temperature PL spectrum for 1.66 eV excitation for comparison.

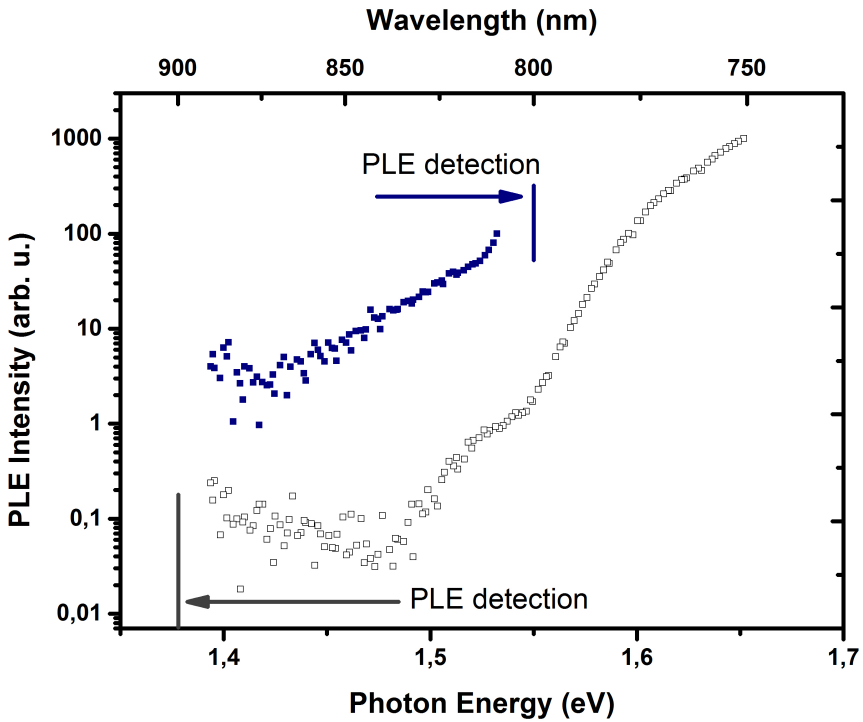


Figure 4.14: 4 K PLE spectra of n-doped InP nanowires (sample IV in Fig. 4.4) with PLE detection below and above the exciting laser, respectively.

white line, where the laser line was deleted from the graphs. Luminescence above those white lines corresponds to photon downconversion and luminescence below to photon upconversion.

In contrast to the results on nanowires (Fig. 4.9) the 4 K downconversion in n-doped bulk InP does not show a clear decrease of luminescence intensity right below the laser energy (see Fig. 4.13 (a) and Fig. 4.10 (a)). Additionally, the clear change of the upconversion PL in n-doped bulk InP (see Fig. 4.13 (b) and (c), and Fig. 4.10 (b)) was not observed for nanowires. Those differences indicate that, while hole scattering in nanowires may be dominated by optical phonon scattering, in bulk material it is dominated by a different scattering mechanism, for example scattering with other charge carriers or acoustic phonons.

4.4 Photon Upconversion in n-doped InP

In Figure 4.4, I presented PLE measurements to show that band-to-band absorption far below the Fermi energy is possible in nanowires even at liquid helium cryostat temperatures. The existence of such absorption and the emission of photons with higher energies than the exciting laser allows the measurement of PLE intensity above the varying laser energy. Figure 4.14 shows a comparison of nanowire PLE signal for detection of the luminescence below (at 1.38 eV) and above (at 1.55 eV) the exciting laser. The first mentioned detection window lies below the bulk InP band gap and detects primarily photons from transitions between states close to the Γ -point of the renormalized band gap. The latter detection window lies close to the luminescence maximum and since it detects above the laser energy, according to the previous discussion it detects only recombinations with holes, that have scattered to higher k -values.

The offset in Figure 4.14 was added to distinguish between up- and down-conversion. The detected luminescence intensity around 1.5 eV was comparable for both measurements, but for upconversion PLE a 5 times longer integration time was used. The two spectra exhibit quite different spectral dependences, which could be attributed to the different mechanisms leading to the detected luminescence. The room temperature PLE measurements on n-doped bulk InP (Fig. 4.13 (d)) show how strongly the PLE spectrum depends on the detection energy.

The fast recombination rate in degenerately doped InP causes a strong dependence of the detected PLE intensity on the hole scattering mechanism and on the energy of the photoexcited hole relative to the detection energy. The PLE spectrum that most closely represents the absorption is obtained by integrating the total emission spectrum for every excitation energy. Such an integrated PLE spectrum of n-doped bulk InP is included in Figure 4.13 (d). The differences between upconversion and downconversion PLE are caused by the different scattering rates to the k -vectors involved in the radiative recombination of electrons and holes.

The fundamental differences between upconversion and downconversion PL can be studied by comparing the excitation intensity dependences of the integrated luminescence intensities with the theoretical dependences derived in Chapter 2.4. In Figure 4.15 the excitation intensity dependence of the integrated upconversion and downconversion intensities for n-doped InP nanowires are shown. For the highest laser intensities the luminescence intensity saturated, which may be caused by the limited number of available conduction band states below the Fermi energy.

For laser intensities below the saturation both upconversion and down-

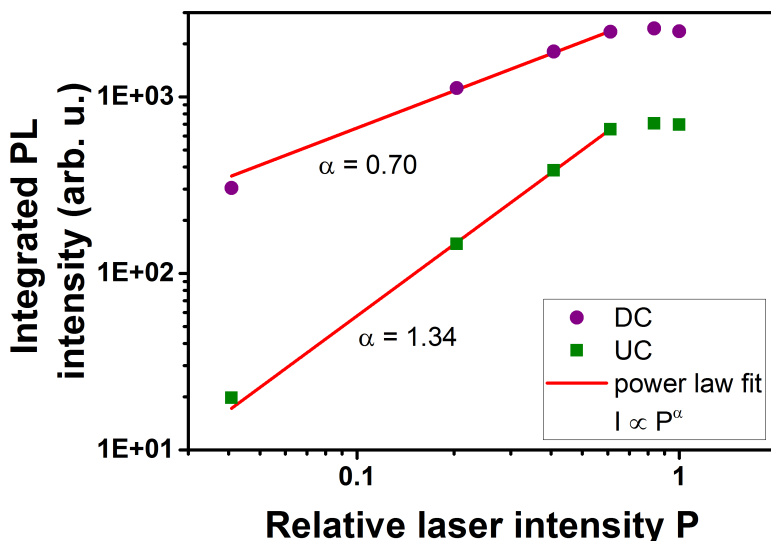


Figure 4.15: Excitation intensity dependence of integrated upconversion (UC) and downconversion (DC) intensity of n-doped InP nanowires for 840 nm (1.48 eV) laser excitation, measured at 4 K.

conversion intensity exhibit a power law dependence, but with different exponents. For photon downconversion the exponent was determined to be around 0.7, while for upconversion an exponent of 1.34 was determined. A power law dependence with exponent $\alpha < 1$ is usually attributed to Auger generation-recombination processes and an exponent $\alpha > 1$ to Shockley-Read-Hall processes. Thus, we assume the detected photon downconversion shows predominately Auger effect heating of the electron gas and the detected photon upconversion is shaped by the non-radiative scattering of holes to higher k -values.

4.5 Photon Upconversion in GaAs

The upconversion mechanism discussed in the previous sections requires only degenerate doping of a direct bandgap semiconductor and unoccupied

4.5 Photon Upconversion in GaAs

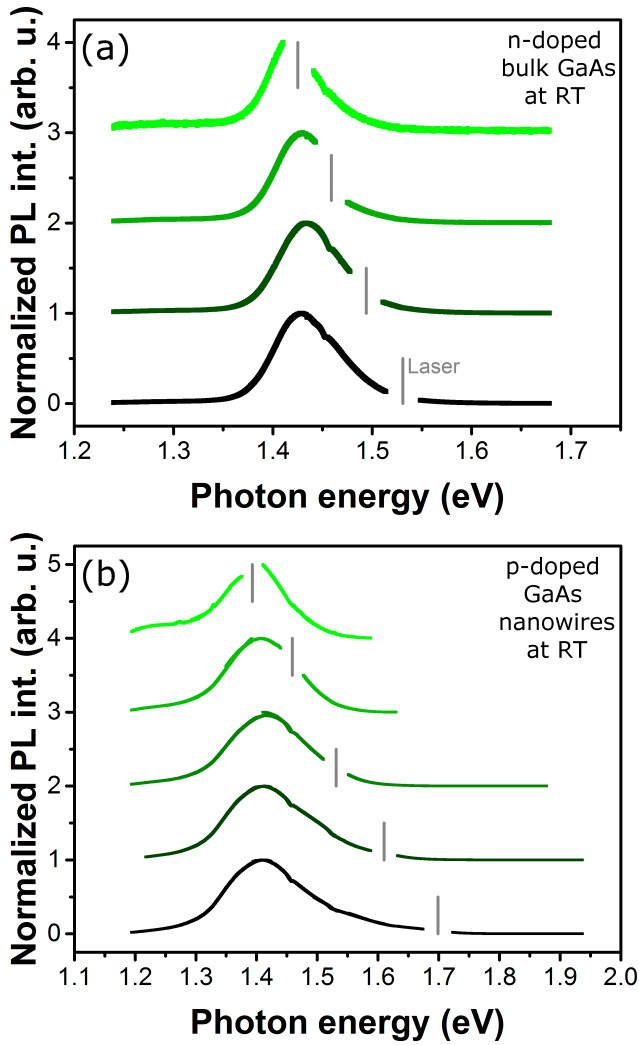


Figure 4.16: Room temperature excitation energy dependence of the normalized luminescence of (a) n-doped bulk GaAs samples and (b) p-doped GaAs nanowires grown by the Aerotaxy method [101]. The excitation laser energy is indicated by vertical gray lines.

Chapter 4: Results

states below the Fermi energy which could be due to elevated sample temperature or due to direct heating of the electron gas. Thus, the upconversion process should not be an n-InP specific attribute. To test the validity of this claim, degenerately n-doped bulk GaAs sample and degenerately p-doped GaAs nanowires were measured and the resulting room temperature PL spectra are presented in Figure 4.16.

In both systems we observe strong photon upconversion at room temperature, which lets us conclude that photon upconversion may have a strong contribution to the optical properties of many degenerately doped direct band semiconductors. Further measurements may reveal if the recombination and scattering processes differ for different materials, dopants and crystal structures.

Chapter 5

Conclusion and Outlook

*"We demand rigidly defined areas of doubt and uncertainty!"
Douglas Adams in "The Hitchhiker's Guide to the Galaxy"*

In this thesis, I demonstrated how photoluminescence measurements on degenerately doped semiconductors allow an estimation of the doping concentration without need for electrical contacts. The degenerate doping can furthermore reveal the conduction band structure for energies higher than the bandgap, which we exploited to experimentally support the theoretically predicted existence of a second conduction band minimum in wurtzite InP.

Our luminescence study on degenerately doped InP nanowires revealed a novel photon upconversion mechanism for excitation energies higher than the bandgap, but lower than the Fermi energy. The most important findings of our detailed study of the photon upconversion in n-doped InP nanowires and n-doped bulk InP can be summarized as follows:

- There is significant photon upconversion for $E_g < E_{\text{excitation}} < E_F$.
- The radiative recombination is strongly dominated by \mathbf{k} -conserving vertical transitions.
- The charge carrier recombination rate is higher than or comparable to the scattering rate.

Our proposed mechanism for the observed photon upconversion in degenerately doped InP, includes an elevated electron gas temperature, scattering of the photoexcited holes to higher k -values and \mathbf{k} -conserving vertical transitions of the holes with conduction band electrons with similar \mathbf{k} -vector.

Chapter 5: Conclusion and Outlook

The elevated electron gas temperature allows absorption of photons with energies much lower than the Fermi energy. The electron gas heating may be induced by an elevated sample temperature or by direct heating of the electron gas.

The focus of this thesis was on n-doped InP, but the included first measurements on degenerately n-doped bulk GaAs and degenerately p-doped GaAs nanowires suggest that the mechanism is more common and that similar photon upconversion could be observed as well in other degenerately doped direct band semiconductors.

The upconversion results presented in this work may lead to devices based on low power upconversion. The upconversion mechanism may be used for laser cooling and the understanding of the process may allow a more accurate description of the radiative processes in semiconductors, which may influence the design of optoelectronic devices.

As continuation of the work it would be interesting to study the photon upconversion in degenerately doped GaAs in more detail and extend the study to other direct bandgap semiconductors such as GaN or ZnO. Further experiments should also investigate the time-dependence of the downconversion and upconversion processes and investigate the luminescence at the same energy as the exciting laser photons.

Acknowledgements

So far this thesis was about the scientific results of my time in Lund, but it is unfair that there is only my name on the front page. There should be so many more. I will illustrate that by describing a day at work. A day that never happened, but could have happened:

I get up, drink my coffee, bike to work and go to my office. I pass the first office I had here in Lund, the office I shared with David, Olof and Roslin. That was a good time. I remember when Gerben came down from time to time and we discussed the weirdest topics. I continue to my current office. At the end of my PhD time I will share office with Rong and Maryam, but now I share it with Sofia, which I did for many years. Sharing office with Sofia is great and not only because I am always informed about all the important things that are going on or going to happen.

Sofia is not here yet and I start my computer. Suddenly I get an error message, so I go to Bengt B.'s office for help. Later it would have been Janne or Johanna M., but anyway, Bengt tells me to leave my computer with him so he can have a look at it. Now that I don't have a computer I decide to start a bit earlier than planned with my measurements. In the lab I notice the vacuum pump is broken and somehow the laser is miss-aligned. I try to find Søren. On the way to his office I meet Håkan, George, Ricardo and Waldomiro talking about the important football match in the evening and Håkan tells me that Bengt M. is in his office, but Søren I would find in the workshop. Søren looks at the pump and tells me he would need thirty minutes to repair it.

My next task is to find out what happened to the setup. I talk to David, Neimantas and Dan and somehow we end up fixing the setup together. Yesterday the setup was working and we have no clues who could have changed anything. It probably was the lab troll. When Johanna T. taught me the setup she already said to always check if everything is in place, but we could never prove the troll's existence.

When we are done with the alignments Søren comes with the fixed vacuum pump and I can start my measurements. Today I have two samples. The first sample is an aerotaxy sample I got from Fangfang and Wondwosen. After a while Martin is coming, curious about the latest results. He notices that the peak energy does not fit for GaAs. I find out that the thermal contact of the sample is not good enough. After I fixed it the results look much better.

Now it is time for lunch, but after that the next sample is waiting. The second sample is a sample grown by Jesper and Sebastian. It is a very nice sample. I make sure I measure everything correctly, but when I'm done with

the measurements the results look weird. It could be that... , Mats-Erik will know if that is a possible explanation. He is good at challenging theories and with challenging theories. I meet him in the corridor talking to Lars.

I explain my results and conclusions and Lars directly has some further ideas of interesting things to look for in the results and for more measurements I should do. After a long discussion with Lars and Mats-Erik about the theory, I need some time to digest the new ideas.

On the way to my office Mona tells me I should talk to Knut, but not today because right now he is busy being prefect. Knut was my first contact person here in Lund and helped me a lot settle down here in Sweden. I wonder what he wants to talk about.

When I come to my office Sofia is talking on the phone about renting a gym for the upcoming Fun in Fysicum tournament. That reminds me that we need to call for a FiF meeting to go through the final planing of the tournament. Luckily Bengt has fixed my computer and I can write a mail to Cassie, David, Maciek, Maria, Elin, Francesc, Holger, Daniel and Sofia to call for a meeting. And, I send a mail to invite everyone at Fysicum to come the tournament. Maybe not everyone has seen the posters we put up.

After that Sofia tells me I should write something scientific, because she is out of chocolate, but that has to wait till tomorrow, now it is time for Innebandy. Today we are many players: Anil, Kristian, Gustav, Daniel, Nicklas, Phil, Neimantas, Claes, Magnus and Knut have signed up. It is good we are so may, because I feel still a bit sore from the last match of the "Minority Carriers".

When I come home I have some relaxing time with my family before we have dinner and the kids go to bed. What a busy day. I almost met all my supervisors: Mats-Erik, Lars, Knut and Martin.

That example day illustrates only slightly how many fantastic people I met during my time in Lund. And there are many more than the names mentioned in the text. I thank all of you! You helped me a lot and made it a great time.

Einen riesigen Dank auch an meine Eltern, Geschwister und langjährigen Freunde. Was sind schon räumliche Distanzen, bei so viel Unterstützung und Anteilnahme.

Und der allerherzlichste Dank gilt meiner eigenen kleinen Familie. Zuhause ist, wo ihr seid.

Bibliography

- [1] I. Ferain, C. A. Colinge, and J.-P. Colinge. Multigate transistors as the future of classical metal-oxide-semiconductor field-effect transistors. *Nature*, 479(7373):310–316, 2011.
- [2] J. Wallentin, N. Anttu, D. Asoli, M. Huffman, I. Åberg, M. H. Magnusson, G. Siefert, P. Fuss-Kailuweit, F. Dimroth, B. Witzigmann, H. Q. Xu, L. Samuelson, K. Deppert, and M. T. Borgström. InP nanowire array solar cells achieving 13.8 % efficiency by exceeding the ray optics limit. *Science*, 339:1057–1060, 2013.
- [3] N. Anttu and H. Q. Xu. Coupling of light into nanowire arrays and subsequent absorption. *Journal of nanoscience and nanotechnology*, 10(11):7183–7187, 2010.
- [4] C. P. T. Svensson, T. Mårtensson, J. Trägårdh, C. Larsson, M. Rask, D. Hessman, L. Samuelson, and J. Ohlsson. Monolithic GaAs/InGaP nanowire light emitting diodes on silicon. *Nanotechnology*, 19(30):305201, 2008.
- [5] M. H. Magnusson, B. J. Ohlsson, M. T. Björk, K. A. Dick, M. T. Borgström, K. Deppert, and L. Samuelson. Semiconductor nanostructures enabled by aerosol technology. *Frontiers of Physics*, 9(3):398–418, 2014.
- [6] P. Caroff, M. E. Messing, B. M. Borg, K. A. Dick, K. Deppert, and L.-E. Wernersson. InSb heterostructure nanowires: MOVPE growth under extreme lattice mismatch. *Nanotechnology*, 20(49):495606, 2009.
- [7] B. E. Cohen. Beyond fluorescence. *Nature*, 467:407–408, 2010.
- [8] T. Kostiuik M. M. Abbas and K. W. Ogilvie. Infrared upconversion for astronomical applications. *Applied Optics*, 15(4):961–970, 1976.

- [9] J. D. Bhawalkar, G. S. He, C.-K. Park, C. F. Zhao, G. Ruland, and P. N. Prasad. Efficient, two-photon pumped green upconverted cavity lasing in a new dye. *Optics Communications*, 124(1-2):33–37, 1996.
- [10] Z. Gan, X. Wu, G. Zhou, J. Shen, and P. K. Chu. Is there real upconversion photoluminescence from graphene quantum dots? *Advanced Optical Materials*, 1:554–558, 2013.
- [11] J. E. Stehr, S. L. Chen, N. Koteeswara Reddy, C. W. Tu, W. M. Chen, and I. A. Buyanova. Turning ZnO into an efficient energy upconversion material by defect engineering. *Advanced Optical Materials*, 24:3760–3764, 2014.
- [12] I. V. Ignatiev, I. E. Kozin, H.-W. Ren, S. Sugou, and Y. Masumoto. Anti-stokes photoluminescence of InP self-assembled quantum dots in the presence of electric current. *Physical Review B*, 60: R14001–R14004, 1999.
- [13] P. P. Paskov, P.-O. Holtz, B. Monemar, J. M. Garcia, W. V. Schoenfeld, and P. M. Petroff. Optical up-conversion processes in InAs quantum dots. *Japanese Journal of Applied Physics*, 40:2080–2083, 2001.
- [14] W. Seidel, A. Titkov, J. P. Andre, P. Voisin, and M. Voos. High-efficiency energy up-conversion by an "Auger Fountain" at an InP-AlInAs type-II heterojunction. *Physical Review Letters*, 73(17): 2356–2359, 1994.
- [15] A. Vinattieri, J. Shah, T. C. Damen, and D. S. Kim. Exciton dynamics in GaAs quantum wells under resonant excitation. *Physical Review B*, 50(15):10868, 1994.
- [16] Z. Chine, B. Piriou, M. Oueslati, T. Boufaden, and B. El Jani. Anti-stokes photoluminescence of yellow band in GaN: Evidence of two-photon excitation process. *Journal of Luminescence*, 82(1):81 – 84, 1999.
- [17] S. L. Chen, J. Stehr, N. Koteeswara Reddy, C. W. Tu, W. M. Chen, and I. A. Buyanova. Efficient upconversion of photoluminescence via two-photon absorption in bulk and nanorod ZnO. *Applied Physics B*, 108(4):919–924, 2012.
- [18] P. Y. Yu and M. Cardona. *Fundamentals of Semiconductors*. Springer, Berlin, 2005. ISBN 3-540-25470-6.

- [19] S. M. Sze. *Semiconductor Devices, Physics and Technology*. John Wiley & Sons., New York, 1985. ISBN 0-471-87424-8.
- [20] M. Grundmann. *The physics of semiconductors*. Springer, Berlin, 2006. ISBN 978-3-540-25370-9.
- [21] E. Burstein. Anomalous optical absorption limit in InSb. *Physical Review*, 93:632, 1954.
- [22] T. S. Moss. The interpretation of the properties of indium antimonide. *Proceedings of the Physical Society B*, 76:775, 1954.
- [23] R. Schwabe, A. Haufe, V. Gottschalch, and K. Unger. Photoluminescence of heavily doped n-InP. *Solid State Communications*, 58:485–491, 1986.
- [24] J. Wallentin, K. Mergenthaler, M. Ek, L. R. Wallenberg, L. Samuelson, K. Deppert, M.-E. Pistol, and M. T. Borgström. Probing the wurtzite conduction band structure using state filling in highly doped InP nanowires. *Nano Letters*, 11:2286–2290, 2011.
- [25] F. Yang, M. E. Messing, K. Mergenthaler, M. Ghasemi, J. Johansson, L. R. Wallenberg, M.-E. Pistol, K. Deppert, L. Samuelson, and M. H. Magnusson. Zn-doping of GaAs nanowires grown by Aerotaxy. *Journal of Crystal Growth*, 414:181–186, 2015.
- [26] J. Shah. *Ultrafast spectroscopy of semiconductors and semiconductor nanostructures*. Springer, Berlin, 1996.
- [27] D. Olego and M. Cardona. Photoluminescence in heavily doped GaAs. i. temperature and hole-concentration dependence. *Physical Review B*, 22:886–893, 1980.
- [28] J. De-Sheng, Y. Makita, K. Ploog, and H. J. Queisser. Electrical properties and photoluminescence of Te-doped GaAs grown by molecular beam epitaxy. *Journal of Applied Physics*, 53(2):999–1006, 1982.
- [29] G.-C. Jiang. Low-temperature photoluminescence of sulfur- and magnesium-doped InGaP epilayers grown by liquid-phase epitaxy. *Journal of Applied Physics*, 79:2060, 1996.

- [30] M. K. Hudait, P. Modak, and S. B. Krupanidhi. Si incorporation and burstein-moss shift in n-type GaAs. *Materials Science and Engineering*, B56:1–11, 1999.
- [31] S. B. Nam, D. C. Reynolds, C. W. Litton, T. C. Collins, P. J. Dean, and R. C. Clarke. Free-exciton energy spectrum in inp in a magnetic field. *Physical Review B*, 13:1643–1648, 1976.
- [32] S. B. Nam, D. C. Reynolds, C. W. Litton, R. J. Almassy, T. C. Collins, and C. M. Wolfe. Free-exciton energy spectrum in gaas. *Physical Review B*, 13:761–767, 1976.
- [33] E. F. Schubert. *Doping in III-V semiconductors*. Cambridge Univ. Press, Cambridge, 1993. ISBN 0521419190.
- [34] F. Urbach. The long-wavelength edge of photographic sensitivity and of the electronic absorption of solids. *Physical Review*, 92:1324–1324, 1953.
- [35] S. L. Chuang. *Physics of Optoelectronic Devices*. John Wiley & Sons, Inc, New York, 1995. ISBN 0-471-10939-8.
- [36] J.-B. Wang, D. Ding, S. R. Johnson, S.-Q. Yu, and Y.-H. Zhang. Determination and improvement of spontaneous emission quantum efficiency in gaas/algaas heterostructures grown by molecular beam epitaxy. *Physica Status Solidi B*, 244:2740–2751, 2007.
- [37] F. Auzel. Upconversion and anti-stokes processes with f and d ions in solids. *Chemical Reviews*, 104:139–173, 2004.
- [38] J. I. Pankove. *Optical processes in semiconductors*. Dover, New York, 1975.
- [39] A. Mooradian and G. B. Wright. First order raman effect in III-V compounds. *Solid State Communications*, 4(9):431 – 434, 1966.
- [40] F. Vallée. Time-resolved investigation of coherent LO-phonon relaxation in III-V semiconductors. *Physical Review B*, 49:2460–2468, 1994.
- [41] J. J. Letcher, K. Kang, D. G. Cahill, and D. D. Dlott. Effects of high carrier densities on phonon and carrier lifetimes in Si by time-resolved anti-Stokes Raman scattering. *Applied Physics Letters*, 90(25):252104, 2007.

- [42] M. R. Brown, H. Thomas, J. M. Williams, R. J. Woodward, and W. A. Shand. Experiments on Er^{3+} in SrF_2 . III. coupled-ion effects. *The Journal of Chemical Physics*, 51:3321–3327, 1969.
- [43] F. Auzel. Spectral narrowing of excitation spectra in n-photons up-conversion processes by energy transfers. *Journal of Luminescence*, 31-32:759 – 761, 1984.
- [44] F. Wang and X. Liu. Recent advances in the chemistry of lanthanide-doped upconversion nanocrystals. *Chemical Society Reviews*, 38:976–989, 2009.
- [45] E. Poles, D. C. Selmarten, O. I. Mičić, and A. J. Nozik. Anti-stokes photoluminescence in colloidal semiconductor quantum dots. *Applied Physics Letters*, 75(7):971–973, 1999.
- [46] Y. P. Rakovich, S. A. Filonovich, M. J. M. Gomes, J. F. Donegan, D. V. Talapin, A. L. Rogach, and A. Eychmüller.
- [47] C. Kammerer, G. Cassabois, C. Voisin, C. Delalande, Ph. Roussignol, and J.M. Gérard. Anti-stokes photoluminescence in self-assembled InAs/GaAs quantum dots. *Physica Status Solidi A*, 190(2):505–509, 2002.
- [48] A. Yamamoto, T. Sasao, T. Goto, K. Arai, H.-Y. Lee, H. Makino, and T. Yao. Anti-stokes photoluminescence in CdSe self-assembled quantum dots. *Physica Status Solidi C*, 0(4):1246–1249, 2003.
- [49] J. Diener, D. Kovalev, H. Heckler, G. Polisski, N. Künzner, F. Koch, A. L. Efros, and M. Rosen. Strong low-temperature anti-stokes photoluminescence from coupled silicon nanocrystals. *Optical Materials*, 17(1-2):135 – 139, 2001.
- [50] F. A. J. M. Driessen. High-efficiency energy up-conversion at GaAs-GaInP_2 interfaces. *Applied Physics Letters*, 67(19):2813–2815, 1995.
- [51] H. M. Cheong, B. Fluegel, M. C. Hanna, and A. Mascarenhas. Photoluminescence up-conversion in $\text{GaAs}/\text{Al}_x\text{Ga}_{1-x}\text{As}$ heterostructures. *Physical Review B*, 58:R4254–R4257, 1998.
- [52] H. M. Cheong, D. Kim, M. C. Hanna, and A. Mascarenhas. Effect of doping on photoluminescence upconversion in $\text{GaAs}/\text{Al}_x\text{Ga}_{1-x}\text{As}$ heterostructures. *Applied Physics Letters*, 81(1):58–60, 2002.

- [53] Z. P. Su, K. L. Teo, P. Y. Yu, and K. Uchida. Mechanisms of photoluminescence upconversion at the GaAs/(ordered) GaInP₂ interface. *Solid State Communications*, 99(12):933 – 936, 1996.
- [54] J. Zeman, G. Martinez, P. Y. Yu, and K. Uchida. Band alignment and photoluminescence up-conversion at the GaAs/(ordered)GaInP₂ heterojunction. *Physical Review B*, 55:R13428–R13431, 1997.
- [55] Y.-H. Cho, D. S. Kim, B.-D. Choe, H. Lim, J. I. Lee, and D. Kim. Dynamics of anti-stokes photoluminescence in type-II Al_xGa_{1-x}As-GaInP₂ heterostructures: The important role of long-lived carriers near the interface. *Physical Review B*, 56: R4375–R4378, 1997.
- [56] S. Machida, T. Tadakuma, and K. Fujiwara. Anti-stokes photoluminescence between In_x(Al_{0.17}Ga_{0.83})_{1-x}As/Al_{0.17}Ga_{0.83}As quantum wells with different x values. *Physica E: Low-dimensional Systems and Nanostructures*, 33(1):196 – 200, 2006.
- [57] A. Schindler, R. Bindemann, and K. Kreher. Two-step excitation of photoluminescence in gap. *Physica Status Solidi B*, 59(2):439–445, 1973.
- [58] B. Clerjaud, F. Gendron, and C. Porte. Chromium-induced up conversion in GaP. *Applied Physics Letters*, 38(4):212–214, 1981.
- [59] R. Prasanth, L. K. van Vugt, D. A. M. Vanmaekelbergh, and H. C. Gerritsen. Resonance enhancement of optical second harmonic generation in a ZnO nanowire. *Applied Physics Letters*, 88(18):181501, 2006.
- [60] S.W. Chan, R. Barille, J.M. Nunzi, K.H. Tam, Y.H. Leung, W.K. Chan, and A.B. Djurišić. Second harmonic generation in zinc oxide nanorods. *Applied Physics B*, 84(1):351–355, 2006.
- [61] Y. C. Zhong, K. S. Wong, A. B. Djurišić, and Y. F. Hsu. Study of optical transitions in an individual ZnO tetrapod using two-photon photoluminescence excitation spectrum. *Applied Physics B*, 97(1): 125–128, 2009.
- [62] T. Trupke, M. A. Green, and P. Würfel. Improving solar cell efficiencies by up-conversion of sub-band-gap light. *Journal of Applied Physics*, 92(7):4117–4122, 2002.

- [63] A. Dobrovolsky, S. Sukritanon, Y. Kuang, C. W. Tu, W. M. Chen, and I. A. Buyanova. Energy upconversion in GaP/GaN core/shell nanowires for enhanced near-infrared light harvesting. *Small*, 10(21): 4403–4408, 2014.
- [64] G. Sun, R. Chen, Y. J. Ding, and J. B. Khurgin. Upconversion due to optical-phonon-assisted anti-stokes photoluminescence in bulk GaN. *ACS Photonics*, 2(5):628–632, 2015.
- [65] E. J. Johnson, J. Kafalas, R. W. Davies, and W. A. Dyes. Deep center EL2 and anti-stokes luminescence in semi-insulating GaAs. *Applied Physics Letters*, 40(11):993–995, 1982.
- [66] L. G. Quagliano and H. Nather. Up conversion of luminescence via deep centers in high purity GaAs and GaAlAs epitaxial layers. *Applied Physics Letters*, 45(5):555–557, 1984.
- [67] S. K. Brierley, H. T. Hendriks, W. E. Hoke, P. J. Lemonias, and D. G. Weir. Observation of boron-related photoluminescence in GaAs layers grown by molecular beam epitaxy. *Applied Physics Letters*, 63(6): 812–814, 1993.
- [68] T. Iino. Upconversion photoluminescence in GaAs. *Oyobuturi*, 65(2): 158–162, 1996.
- [69] S. G. Grubb, K. W. Bennett, R. S. Cannon, and W. F. Humer. CW room-temperature blue upconversion fibre laser. *Electronics Letters*, 28 (13):1243–1244, 1992.
- [70] Z. Li, Y. Zhang, and S. Jiang. Multicolor core/shell-structured upconversion fluorescent nanoparticles. *Advanced Materials*, 20(24): 4765–4769, 2008.
- [71] J. Zhang, D. Li, R. Chen, and Q. Xiong. Laser cooling of a semiconductor by 40 kelvin. *Nature*, 493:504–508, 2013.
- [72] C. M. Wolfe, G. E. Stillman, and W. T. Lindley. Electron mobility in high-purity GaAs. *Journal of Applied Physics*, 41(7):3088–3091, 1970.
- [73] T. Brudevoll, T. A. Fjeldly, J. Baek, and M. S. Shur. Scattering rates for holes near the valence-band edge in semiconductors. *Journal of Applied Physics*, 67(12):7373–7382, 1990.

- [74] A. Chébir, J. Chesnoy, and G. M. Gale. Femtosecond relaxation of photoexcited holes in bulk gallium arsenide. *Physical Review B*, 46: 4559–4563, 1992.
- [75] P. Langot, R. Tommasi, and F. Vallée. Nonequilibrium hole relaxation dynamics in an intrinsic semiconductor. *Physical Review B*, 54: 1775–1784, 1996.
- [76] J. R. Lowney and H. S. Bennett. Majority and minority electron and hole mobilities in heavily doped GaAs. *Journal of Applied Physics*, 69 (10):7102–7110, 1991.
- [77] T. Terashige, H. Yada, Y. Matsui, T. Miyamoto, N. Kida, and H. Okamoto. Temperature and carrier-density dependence of electron-hole scattering in silicon investigated by optical-pump terahertz-probe spectroscopy. *Physical Review B*, 91:241201, 2015.
- [78] M. Combescot and R. Combescot. Conductivity relaxation time due to electron-hole collisions in optically excited semiconductors. *Physical Review B*, 35:7986–7992, 1987.
- [79] J. Czochralski. Ein neues Verfahren zur Messung der Kristallisationsgeschwindigkeit der Metalle. *Zeitschrift für physikalische Chemie*, 92:219–221, 1918.
- [80] J. E. Clemans, T. I. Ejim, W. A. Gault, and E. M. Monberg. Bulk III-V compound semi-conductor crystal growth. *AT T Technical Journal*, 68 (1):29–42, 1989.
- [81] K. L. Choy. Chemical vapour deposition of coatings. *Progress in Materials Science*, 48:57 – 170, 2003.
- [82] K. Mergenthaler, V. Gottschalch, J. Bauer, H. Paetzelt, and G. Wagner. Growth and characterization of ZnO nanostructures on sapphire substrates. *Journal of Crystal Growth*, 310(23):5134 – 5138, 2008.
- [83] K. A. Dick. A review of nanowire growth promoted by alloys and non-alloying elements with emphasis on au-assisted III-V nanowires. *Progress in Crystal Growth and Characterization of Materials*, 54(3-4): 138–173, 2008.
- [84] R. S. Wagner and W. C. Ellis. Vapor-liquid-solid mechanism of single crystal growth. *Applied Physics Letters*, 4(5):89–90, 1964.

- [85] A. V. Kuhlmann, J. Houel, D. Brunner, A. Ludwig, D. Reuter, A. D. Wieck, and R. J. Warburton. A dark-field microscope for background-free detection of resonance fluorescence from single semiconductor quantum dots operating in a set-and-forget mode. *Review of Scientific Instruments*, 84:073905, 2013.
- [86] R. E. Algra, M. A. Verheijen, M. T. Borgström, L.-F. Feiner, G. Immink, W. J. P. van Enkevort, E. Vlieg, and E. P. A. M. Bakkers. Twinning superlattices in indium phosphide nanowires. *Nature*, 456(7220): 369–372, 2008.
- [87] J. Wallentin and M. T. Borgström. Doping of semiconductor nanowires. *Journal of Materials Research*, 26(17):2142–2156, 2011.
- [88] C. Thelander, K. A. Dick, M. T. Borgström, L. E. Fröberg, P. Caroff, H. A. Nilsson, and L. Samuelson. The electrical and structural properties of n-type InAs nanowires grown from metal-organic precursors. *Nanotechnology*, 21(20):205703, 2010.
- [89] V. Siklitsky. Physical properties of semiconductors. <http://www.ioffe.rssi.ru/SVA/NSM/Semicond/index.html>. Ioffe Physical Technical Institute, 26 Polytekhnicheskaya, St Petersburg 194021, Russian Federation.
- [90] A. De and C. E. Pryor. Predicted band structures of III-V semiconductors in the wurtzite phase. *Physical Review B*, 81:155210, 2010.
- [91] A. Mishra, L. V. Titova, T. B. Hoang, H. E. Jackson, L. M. Smith, J. M. Yarrison-Rice, Y. Kim, H. J. Joyce, Q. Gao, H. H. Tan, and C. Jagadish. Polarization and temperature dependence of photoluminescence from Zn-blende and wurtzite InP nanowires. *Applied Physics Letters*, 91(26): 263104, 2007.
- [92] G. L. Tuin, M. T. Borgström, J. Trägårdh, M. Ek, L. R. Wallenberg, L. Samuelson, and M.-E. Pistol. Valence band splitting in wurtzite InP nanowires observed by photoluminescence and photoluminescence excitation spectroscopy. *Nano Research*, 4:159–163, 2011.
- [93] I. Vurgaftman, J. R. Meyer, and L. R. Ram-Mohan. Band parameters for III-V compound semiconductors and their alloys. *Journal of Applied Physics*, 89(11):5815–5875, 2001.

- [94] S. Perera, K. Pemasiri, M. A. Fickenscher, H. E. Jackson, L. M. Smith, J. Yarrison-Rice, S. Paiman, Q. Gao, H. H. Tan, , and C. Jagadish. Probing valence band structure in wurtzite InP nanowires using excitation spectroscopy. *Applied Physics Letters*, 97:023106, 2010.
- [95] E. G. Gadret, G. O. Dias, L. C. O. Dacal, M. M. de Lima Jr., C. V. R. S. Ruffo, F. Iikawa, M. J. S. P. Brasil, T. Chiaramonte, M. A. Cotta, L. H. G. Tizei, D. Ugarte, and A. Cantarero. Valence-band splitting energies in wurtzite InP nanowires: Photoluminescence spectroscopy and ab initio calculations. *Physical Review B*, 82:125327, 2010.
- [96] K. Ikejiri, Y. Kitauchi, K. Tomioka, J. Motohisa, and T. Fukui. Zinc blende and wurtzite crystal phase mixing and transition in indium phosphide nanowires. *Nano Letters*, 11:4314–4318, 2011.
- [97] J. Shah. Hot electrons and phonons under high intensity photoexcitation of semiconductors. *Solid-State Electronics*, 21:43–50, 1978.
- [98] C. H. Yang, J. M. Carlson-Swindle, S. A. Lyon, and J. M. Worlock. Hot-electron relaxation in GaAs quantum wells. *Physical Review Letters*, 55(21):2359, 1985.
- [99] R. S. Turtelli, A. R. B. de Castro, and R. C. C. Leite. Single particle scattering from hot electrons in GaAs. *Solid State Communications*, 16(8):969 – 971, 1975.
- [100] T. Trupke, M. A. Green, P. Würfel, P. P. Altermatt, A. Wang, J. Zhao, and R. Corkish. Temperature dependence of the radiative recombination coefficient of intrinsic crystalline silicon. *Journal of Applied Physics*, 94(8):4930–4937, 2003.
- [101] M. Heurlin, M. H. Magnusson, D. Lindgren, M. Ek, L. R. Wallenberg, K. Deppert, and L. Samuelson. Continuous gas-phase synthesis of nanowires with tunable properties. *Nature*, 492(7427):90–94, 2012.